

Single-cell virus sequencing of influenza infections that trigger innate immunity

Alistair B. Russell,^a Elizaveta Elshina,^b Jacob R. Kowalsky,^a Aartjan J. W. te Velthuis,^b Jesse D. Bloom^{a,c,d,*}

^aBasic Sciences and Computational Biology, Fred Hutchinson Cancer Research Center, Seattle, United States

^bDivision of Virology, Department of Pathology, University of Cambridge, Cambridge, United Kingdom

^cDepartment of Genome Sciences, University of Washington, Seattle, United States

^dHoward Hughes Medical Institute, Seattle, United States

Compiled April 26, 2019

This is a draft manuscript, pre-submission

Address correspondence to Jesse D. Bloom,
jbloom@fredhutch.org.

ABSTRACT The outcome of viral infection is extremely heterogeneous, with infected cells only sometimes activating. Influenza-infected cells vary widely in their expression of viral genes, and only occasionally activate innate immunity. Here we develop a new method to assess how the genetic variation in viral populations contributes to this heterogeneity. We do this by determining the transcriptome and full-length sequences of all viral genes in single cells infected with a nominally “pure” stock of influenza virus. Most cells are infected by virions with defects, some of which increase the frequency of innate-immune activation. These immunostimulatory defects are diverse, and include mutations that perturb the function of the viral polymerase protein PB1, large internal deletions in viral genes, and failure to express the virus’s interferon antagonist NS1. However, immune activation remains stochastic in cells infected by virions with these defects, and occasionally is triggered even by virions that express unmutated copies of all genes. Our work shows that the diverse spectrum of defects in influenza virus populations contributes to—but does not completely explain—the heterogeneity in infection outcome, viral gene expression and immune activation in single infected cells.

IMPORTANCE Because influenza virus has a high mutation rate, many cells are infected by mutated virions. But so far, it has been impossible to fully characterize the sequence of the virion infecting any given cell, since conventional techniques like flow cytometry and single-cell RNA-seq only detect if a protein or transcript is present—not its sequence. Here we develop a new approach that uses long-read PacBio sequencing to determine the sequences of virions infecting single cells. We show that viral genetic variation explains some but not all of the cell-to-cell variability in infection outcome, viral gene expression and innate-immune induction. Overall, our study provides the first complete picture of how viral mutations affect the course of infection in single cells.

KEYWORDS: influenza virus; interferon; PacBio; single-cell RNAseq; 10X Chromium; NS1; PB1; defective virus; heterogeneity

INTRODUCTION

Infection with an acute virus such as influenza initiates a race between the virus and immune system. As the virus spreads, some cells detect infection and begin producing interferon (IFN). This IFN directs expression of anti-viral interferon-stimulated genes (ISGs) in the infected cell and its neighbors via autocrine and paracrine signaling, as well as helping launch a broader immune response (1, 2). If innate immunity is activated sufficiently rapidly, it can reduce viral replication and disease (3, 4, 5, 6, 7)—

42 although excessive immune responses later in infection can actually be associated with
 43 immunopathology and severe disease (8, 9).

44 Unfortunately for the host, influenza initially only rarely triggers IFN production by
 45 infected cells (10, 11). This rareness of IFN induction is just one form of the extreme
 46 cell-to-cell heterogeneity that characterizes infection: cells also vary widely in their
 47 production of viral mRNA, proteins, and progeny virions (12, 13, 14, 15, 16). Because
 48 viral growth and the IFN response ~~are both feed-forward processes, early cell-to-cell~~
~~heterogeneity both amplify themselves, early variation in the initiation of these events~~
 49 could have significant downstream consequences for the race between virus and im-
 50 mune system—especially since natural human infections are typically ~~initiated founded~~
 51 by just a few virions entering a few cells (17, 18, 19).

52 It is unclear why only some infected cells trigger innate-immune responses. Two
 53 possible contributors are pure stochasticity and pre-existing variation in cellular state.
 54 For instance, only some cells induce IFN even upon treatment with synthetic innate-
 55 immune ligands (20, 21, 22), and the frequency of IFN induction may depend on a
 56 cell's pre-existing chromatin state (23). But for influenza, a third possible contributor
 57 also looms large: viral genetic diversity. ~~Because~~ The virus has evolved mechanisms to
 58 avoid IFN induction, including expressing proteins that interfere with innate-immune
 59 induction (24, 25, 26, 27, 28) and sequestering immunogenic viral RNA (29). However,
 60 because influenza has a high mutation rate (30, 31, 32, 33, 34), individual virions of-
 61 ten have genetic defects (30, 31, 32, 33, 34) that could impair these immune-evasion
 62 strategies. Indeed, many studies have identified mutations that increase IFN induction
 63 when engineered into a viral population (11, 35, 36, 37), and viral stocks that are rich in
 64 internal deletions in the polymerase genes induce more IFN (16, 38, 39, 40, 41, 42).

65 However, existing techniques are inadequate to determine how viral genetic di-
 66 versity contributes to cell-to-cell heterogeneity during infection. Flow cytometry and
 67 fluorescent reporters only measure protein levels (14, 43, 44), and current single-cell
 68 transcriptomic techniques measure abundance of transcripts and provide only frag-
 69 mentary information on their sequences (12, 13, 16, 45, 46, 47, 48). None of these
 70 techniques reliably reveal if the virion infecting a specific cell has some idiosyncratic
 71 mutation.

72 Here we develop a new approach to measure both the full transcriptome and
 73 sequences of all viral genes in single influenza-infected cells. To do this, we perform
 74 both standard Illumina-based transcriptomics and full-length PacBio sequencing of
 75 viral genes from single cells. Two-thirds of cells are infected by virions that have a
 76 mutation or defect in gene expression. We identify several types of viral defects that
 77 increase IFN induction, but also show that viral diversity is insufficient to fully explain
 78 cell-to-cell heterogeneity during influenza infection.

80 RESULTS

81 **A system to identify and enrich rare IFN+ cells.** Influenza virus only rarely trig-
 82 gers IFN expression in infected cells (11, 12, 10)—a fact that poses a challenge for the
 83 study IFN induction in single cells. Therefore, we developed a method to identify and
 84 enrich rare IFN+ cells by creating A549 cells that carried IFN reporters consisting of a
 85 type I (*IFNB1*) or type III (*IFNL1*) promoter driving expression of a cell-surface protein
 86 (*LNGFRΔC* (49, 50)) followed by a fluorescent protein (Fig. 1A). Cells that activate the
 87 IFN reporters can be enriched by magnetic-activated cell sorting (MACS) or identified
 88 by flow cytometry. The reporters were efficiently activated by infection with a strain of
 89 Sendai virus (51) that potently induces IFN (Fig. S1A), and activation of the type I and
 90 type III IFN reporters was highly correlated in our cells (Fig. S1B; further validated by

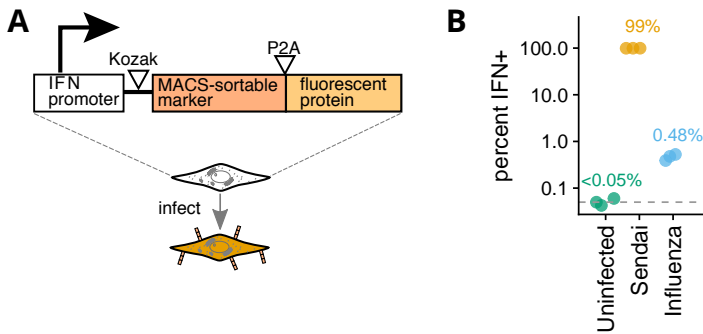


FIG 1 Reporter cells to identify and enrich infections that activate IFN expression. (A) The reporter consists of an IFN promoter that drives expression of a cell-surface protein amenable to MACS and a fluorescent protein. We created reporters with type I and type III IFN promoters (File S1). In A549 cells, the reporters were efficiently activated by an IFN-inducing strain of Sendai virus (Fig. S1A). (B) Frequency of IFN induction upon infection with the influenza virus stock used in the single-cell studies in this paper, as quantified using the type III IFN reporter (see Fig. S2 for full flow cytometry data). The plot also shows uninfected cells, and cells infected with Sendai virus. The limit of detection of 0.05% is indicated with a dashed line, and numbers show the median of three measurements.

91 the single-cell transcriptomics below). Therefore, for the rest of this paper, we use “IFN
92 expression” to refer to combined expression of type I and III IFNs.

93 We generated a stock of A/WSN/1933 (H1N1) influenza (hereafter referred to as
94 “WSN”) directly from reverse-genetics plasmids (52), and passaged this stock at low
95 multiplicity of infection (MOI). This process ensures that the viral stock that is relatively
96 “pure”, with only low levels of the large internal deletions and other defects that arise
97 in stocks passaged at high MOI (53). As described in the next subsection, our stock
98 actually consisted of a mix of two viruses: wild-type WSN and a variant of this virus
99 that carries synonymous viral “barcodes” near the termini of each gene. This viral
100 stock activated the IFN reporter in ~0.5% of infected cells (Fig. 1B), a frequency roughly
101 comparable to that reported in prior studies (11, 12). We also validated that MACS for
102 the cell-surface protein driven by the IFN reporter enriched the IFN+ cells by >50-fold
103 (Fig. S3).

104 **Combined transcriptomics and virus-sequencing of single infected cells.** We
105 developed the approach in Fig. 2 to obtain the entire transcriptome *and* the full se-
106 quences of all viral genes in single cells. First, we generated the viral stock described
107 in the previous subsection, which consisted of a mix of wild-type WSN and a “syn-
108 onymously barcoded” variant that contained two engineered synonymous mutations
109 near each termini of each gene (File S2). These viral barcodes allow us to identify
110 co-infections from single-cell transcriptomic data (12), and provide a control for PCR
111 artifacts during full-length sequencing of viral transcripts (see below). We used this
112 viral stock to infect A549 IFN reporter cells (Fig. 2A) at a dose that led to detectable
113 viral transcription in ~25% of cells (this moderately low MOI reasonably balances our
114 desire to limit the number of co-infections with the cost of performing transcriptomics
115 on uninfected cells). From 12 to 13 hours post-infection, we used MACS to enrich cells
116 that activated the IFN reporter. To ensure the presence of IFN-IFN-negative cells, we
117 added back non-enriched cells to ~10% of the total. We also added uninfected canine
118 cells to ~5% of the total as a control for multiplets and to estimate the background
119 amount of viral mRNA detected in truly uninfected cells.

120 We processed the cells on a commercially available platform (54) that isolates cells

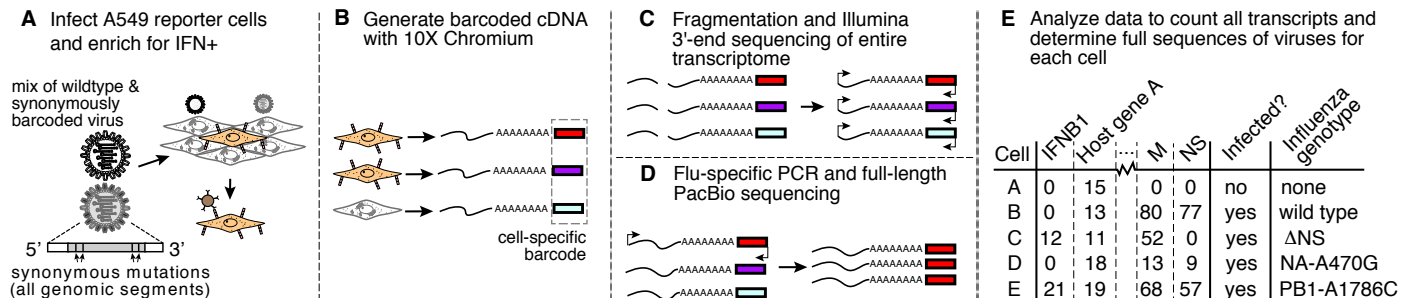


FIG 2 Approach for combined transcriptomics and viral sequencing of single influenza-infected cells that express IFN. (A) IFN reporter A549 cells are infected with a mix of wild-type and synonymously barcoded viruses. IFN+ cells are enriched by MACS, and pooled with non-enriched cells and uninfected canine cells that serve as a control for multiplets and mRNA leakage. (B) The mRNAs from individual cells are converted to cDNAs tagged with cell-specific barcodes. (C) Cellular transcriptomes are quantified using standard single-cell 3'-end Illumina sequencing, and (D) viral genes are enriched by influenza-specific PCR and fully sequenced by PacBio (in this schematic, only the cell labeled by the red barcode is infected and has viral transcripts that are sequenced by PacBio). (E) The result is a matrix giving the expression of each gene in each cell, as well as the full sequences of the viral genes in infected cells.

in droplets and reverse transcribes polyadenylated mRNAs to append a unique cell barcode to all cDNAs in each droplet, and a unique molecular identifier (UMI) to each cDNA molecule (Fig. 2B). Because influenza virus mRNAs are polyadenylated (55), this process appends cell barcodes to viral as well as cellular mRNAs. Furthermore, because virtually the entire influenza genome is transcribed, the cell-barcoded cDNA spans almost all 13,581 nucleotides in the segmented viral genome: the only portions not covered are one universally conserved nucleotide upstream of the transcription start site (56) and 17 to 22 highly conserved nucleotides downstream of the polyadenylation site (55) in each of the eight viral gene segments.

We used a portion of the cell-barcoded cDNA for standard single-cell transcriptomics by Illumina 3'-end sequencing (Fig. 2C). But we also took a portion and enriched for full-length viral molecules by PCR (Fig. 2D). We performed PacBio sequencing on these full-length viral cDNAs to generate high-accuracy circular consensus sequences (CCSs) (57). These CCSs retain the cell barcodes, and with sufficient sequencing depth we obtain CCSs from multiple unique UMI-tagged cDNAs for each viral gene in each cell. Because most cells are infected by just one or two virions, we can build a consensus of CCSs for each viral gene in each cell to determine the sequence(s) of these virions. Combining this information with the 3'-end sequencing determines the entire transcriptome and the full sequences of the infecting virions in single cells (Fig. 2E).

Transcriptomic analyses of single IFN+ and IFN- influenza-infected cells. We obtained transcriptomes for 1,614 human (A549) cells, and 50 of the uninfected canine cells that were spiked into the experiment as a control (Fig. 3A). We also obtained 12 transcriptomes with a mix of human and canine transcripts; from the number of such mixed cell-type transcriptomes, we estimate (58) that ~11% of the transcriptomes are derived from multiple cells. To remove some of these multiplets along with low-quality droplets, we filtered transcriptomes with unusually high or low numbers of cellular transcripts as is commonly done in analysis of single-cell RNA-seq data (59). After this filtering, we retained 1,490 human cells for further analysis (Fig. 3B)

To identify infected cells, we examined the fraction of each transcriptome derived from virus (Fig. 3C). As expected, only a small fraction (~0.7%) of transcripts in the uninfected canine cells were viral; this low-level background is likely from lysed cells that release ambient viral mRNA. We tested whether each cell contained significantly more viral transcripts than expected under a Poisson model given this background

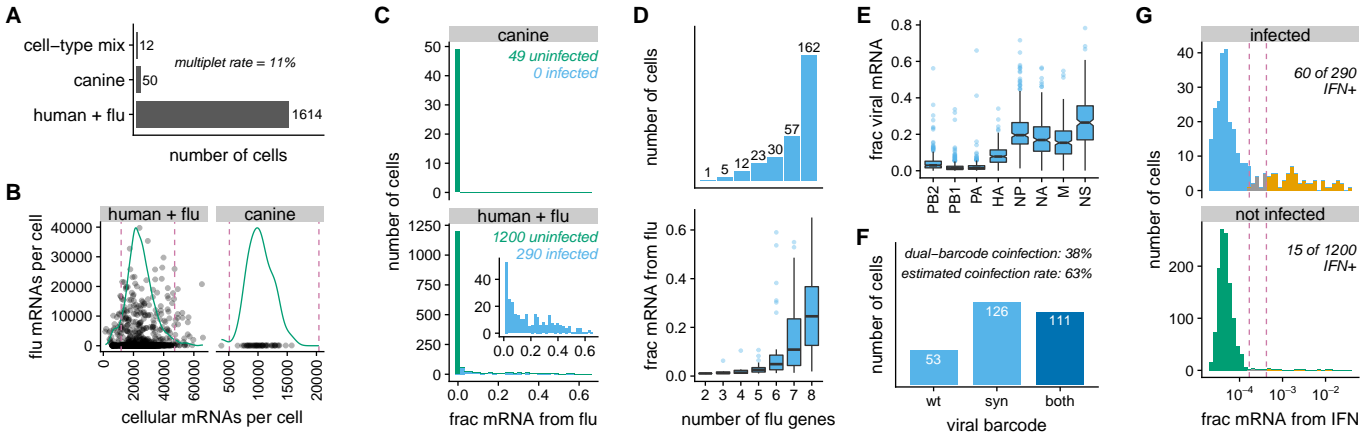


FIG 3 Single-cell transcriptomics of IFN-enriched influenza-infected cells. (A) Number of cells for which transcriptomes were obtained. From these numbers, we estimate (58) that $\approx 11\%$ of the transcriptomes are derived from multiple cells. (B) The number of cellular and viral mRNAs detected for each cell is plotted as a point. Green lines show the distribution of cellular mRNAs per cell. Cells outside the dashed magenta lines have unusually low or high amounts of cellular mRNA (likely low-quality emulsions or multiplets), and are excluded from subsequent analyses. (C) Distribution across cells of the fraction of all mRNA derived from influenza. Cells called as infected are in blue, while other cells are in green. The inset shows the amount of viral mRNA in the human cells that are called as infected. (D) Number of influenza genes detected per infected cell, and the amount of viral mRNA in cells expressing each number of viral genes. Fig. S4 shows the frequency that each viral gene is detected. (E) Relative expression of viral genes, quantified as the fraction of all viral mRNA in each infected cell derived from each gene. (F) Number of cells infected with wild-type virus, synonymously barcoded virus, or both. From the cells infected with both viral barcodes, we estimate (58) that 63% of infected cells are co-infected. (G) Fraction of cellular mRNA from IFN across cells, faceted by whether the cells are infected. Cells to the left of the first dashed magenta line are classified as IFN-, and cells to the right of the second line as IFN+. A pseudocount is added to the number of IFN transcripts detected in each cell, which is why none of the fractions are zero.

fraction, and classified 290 human cells as definitively infected with influenza (Fig. 3C). We classified the other cells as uninfected, although it is possible that some were infected with virions that produced very little mRNA. The distribution of the amount of viral mRNA across infected cells is shown in the inset in Fig. 3C. As in our prior work (12), the distribution is extremely heterogeneous: many infected cells have only a few percent of mRNA derived from virus, but viral mRNA comprises over half the transcriptome of a few cells.

We called the presence or absence of each viral gene in each infected cell, again using a Poisson model parameterized by background fractions estimated from uninfected canine cells. We called presence / absence of genes rather than transcripts, since the two genes that encode multiple transcripts (M1 / M2 from the M gene, and NS1 / NS2 from the NS gene) do so via alternative splicing that leaves both isoforms with the same termini, making them indistinguishable by 3'-end sequencing. Fig. 3D (top panel) shows that 162 of 290 infected cells express all eight genes (see Fig. S4 for frequencies for individual genes). This measured frequency of infected cells expressing all eight genes is slightly higher than in our own prior work using the WSN strain (12), and slightly to substantially higher than that reported in studies by others using different viral strains or methodologies (15, 43, 60, 61).

The amount of viral mRNA was lower in cells that failed to express viral genes (Fig. 3D, bottom panel). However, viral burden remained highly variable even after conditioning on the number of viral genes: some cells that failed to express one or even two genes still derived $>50\%$ of their mRNA from virus, while other cells that expressed all genes had only a few percent of their mRNA from virus (Fig. 3D, bottom panel). Consistent with our prior work (12), despite the wide variation in absolute

178 expression of viral genes, their *relative* expression was fairly consistent (Fig. 3E) and
 179 generally matched values from older bulk studies (62).

180 By examining the synonymous viral barcodes near the 3' termini of transcripts,
 181 we determined that 38% of cells were co-infected with wild-type and synonymously
 182 barcoded virions (Fig. 3F; cells called as co-infected if a binomial test rejected null
 183 hypothesis that $\geq 95\%$ of viral mRNA is from one viral barcode variant). From Fig. 3F,
 184 we estimate (58) that 63% of infected cells are co-infected, implying that 25% are
 185 co-infected with two virions with the same viral barcode (such co-infections cannot be
 186 identified from transcriptomic data). Interestingly, this co-infection rate is higher than
 187 expected from the relative numbers of infected and uninfected cells (Fig. 3C) if infection
 188 is Poisson. This discrepancy could arise if the MACS for IFN+ cells also enriches co-
 189 infected cells, if infection is not truly Poisson, or if co-infection increases complements
 190 otherwise transcriptionally defective virions to increase the likelihood that we identify
 191 a cell as infected given the thresholds in C. This. The first explanation seems unlikely,
 192 as there is no tendency for co-infected cells to express more IFN (Fig. S5). Therefore
 193 we favor the latter two explanations, both of which have been demonstrated for other
 194 viruses (63, 64). The moderately high rate of co-infection may also explain why more
 195 cells in our experiment express all eight viral genes compared to some prior studies,
 196 as a co-infecting virion can complement a missing viral gene.

197 We next examined expression of IFN and ISGs (Fig. 3G and Fig. S6). Over 20%
 198 of infected cells were IFN+, indicating that the MACS successfully enriched IFN+ cells
 199 far beyond their initial frequency. The expression of type I and type III IFN was highly
 200 correlated in single cells, justifying our decision to collapse both classes under the
 201 single label of "IFN" in the analyses that follow (Fig. S7). Few (~1.3%) uninfected
 202 cells were IFN+; the few that were present might be because the MACS enriched
 203 for rare cells that spontaneously activated IFN, activated IFN in response to non-viral
 204 ligands (65, 66, 67) or because some cells that we classified as uninfected were ac-
 205 tually infected at low levels. The difference in the frequency of IFN positivity among
 206 infected and uninfected cells in Fig. 3G was highly significant ($P < 10^{-5}$, Fisher's exact
 207 test). Many more cells expressed ISGs than IFN itself (Fig. S6A). The IFN+ cells were a
 208 subset of the ISG+ cells: IFN+ cells always expressed ISGs, but many ISG+ cells did not
 209 express IFN (Fig. S6B). These results are consistent with the established knowledge that
 210 IFN is expressed only primarily in cells that directly detect infection, but that ISGs are
 211 also expressed via paracrine signaling in other cells (1, 2).

212 Finally, we qualitatively examined how expression of viral genes, IFN, and ISGs
 213 relate to the overall structure of the high-dimensional transcriptomic data. Fig. S8
 214 shows unsupervised t-SNE clustering (68) of the cells. Cells expressing high levels of
 215 viral genes, IFN, and ISGs cluster together—and most of the structure in the t-SNE plot
 216 that is not associated with these genes involves uninfected and IFN- cells.

217 **Full genotypes of viruses infecting single IFN+ and IFN- cells.** We next used
 218 PacBio sequencing (Fig. 2D) to determine the full sequences of the viral genes in single
 219 infected cells. We obtained >200,000 high-quality PacBio CCSs that mapped to an
 220 influenza gene and contained a cell barcode and UMI (Fig. S9). The synonymous viral
 221 barcodes at both termini of each gene enabled us to confirm that PCR strand exchange
 222 was rare (Fig. S10), meaning that the vast majority of CCSs correctly link the sequence
 223 of the transcript to cell barcodes and UMIs that identify the cell and molecule of origin.

224 After calling the presence / absence of each viral gene in each cell as described
 225 in the previous section, we called mutations if they were found in at least two CCSs
 226 originating from different mRNAs (unique UMIs) and at least 30% of all CCSs for that
 227 gene in that cell. For cells co-infected with both viral barcode variants, we called

Single-cell virus sequencing of influenza infections that trigger innate immunity

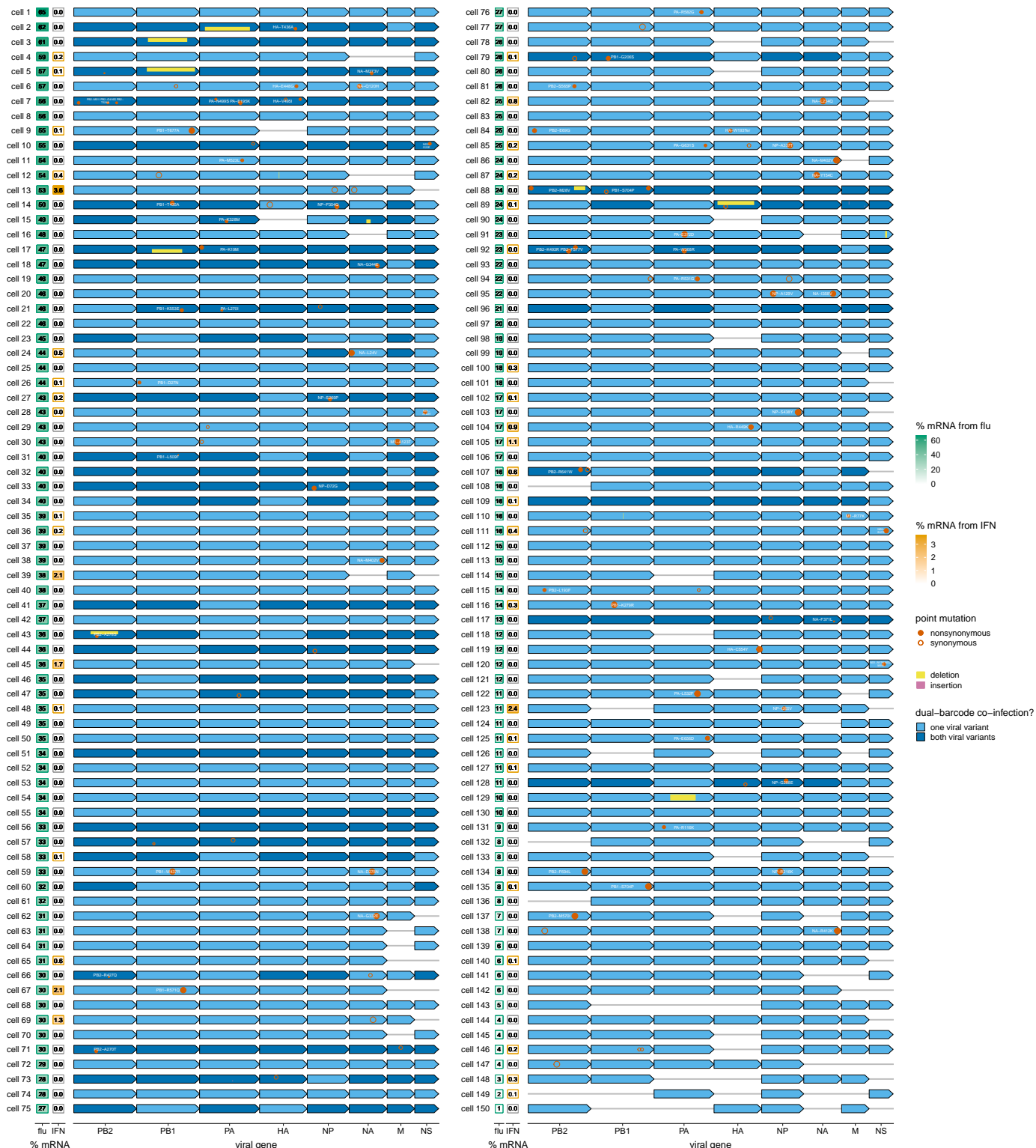


FIG 4 Viral genotypes and infection outcomes in single cells. Green and orange boxes at the left show the percent of all mRNA in that cell derived from virus and the percent of all cellular mRNA derived from IFN, respectively. The second box is framed in orange for cells classified as IFN+ in Fig. 3G. Blue arrows indicate the presence of a viral gene from one (light blue) or both (dark blue) viral barcode variants; a dark blue arrow therefore means that a cell was co-infected. Circles and boxes on the arrows indicate mutations or indels as described in the legend at right. The circle areas and box heights are proportional to the fraction of CCSs with that mutation. For dual-barcode infections, mutations / indels for the wild-type and synonymously barcoded viral variants are shown in the top and bottom half of the arrows, respectively. For instance, cell 5 was co-infected by a virion with one unmutated and one internally deleted copy of PB1.

228 mutations separately for each viral variant. This strategy reliably identifies mutations
 229 in virions that initiate infection of cells infected with at most one virion of each viral
 230 barcode variant (~75% of infected cells), as well as high-abundance mutations in cells
 231 co-infected with multiple virions of the same viral barcode. It will not identify mutations
 232 that arise within a cell after the first few rounds of viral genome replication, since such
 233 mutations will not reach 30% frequency in that cell. Therefore, analogous to somatic
 234 variant calling in tumor sequencing (69, 70), there is a limit to our detection threshold:
 235 we cannot identify mutations that occur on just a small fraction of transcripts in a cell.

236 We could call the sequences of all expressed viral genes in the majority of infected
 237 cells (Fig. S11). We were most effective at calling full viral genotypes in cells that
 238 expressed high amounts of viral mRNA and were infected by only one viral barcode
 239 variant (Fig. S11). But we also called full genotypes for many cells that had low viral
 240 burden or were co-infected by both viral barcode variants.

241 The 150 cells for which we called the full viral genotypes are shown in Fig. 4. Visual
 242 inspection of this figure reveals a wealth of information. For instance, the cell with
 243 the highest viral burden (*cell 1* in Fig. 4, which has 65% of its mRNA from virus) was
 244 infected by a virion that expressed unmutated copies all eight genes and did not induce
 245 detectable IFN. But 12 of the other 13 cells with at least 50% of their mRNA from
 246 virus were infected by virions that had a mutation or failed to express a gene, and
 247 five of these cells produced IFN. As expected, all cells infected by virions that failed to
 248 express a component of the viral polymerase complex (PB2, PB1, PA, or NP) expressed
 249 low amounts of viral mRNA since they are limited to primary transcription off the
 250 incoming proteins (e.g., *cell 132* and *cell 143*). The two cells that expressed the most
 251 IFN (*cell 13* and *cell 123*) lacked the viral NS gene that encodes the virus's primary IFN
 252 antagonist (24, 25). Many other IFN+ cells had different defects such as large internal
 253 deletions (e.g., *cell 5* and *cell 89*) or amino-acid mutations (e.g., *cell 9*, *cell 28*, and many
 254 others).

255 However, Fig. 4 also reveals stochasticity that is independent of viral genotype.
 256 This stochasticity sometimes acts to the detriment of the virus, and sometimes to
 257 the detriment of the cell. As an example of the former case, expressing unmutated
 258 copies of all eight genes did not guarantee a favorable outcome for the virus
high viral
gene expression and successful innate-immune evasion: for instance, the unmutated
 259 virion that infected *cell 139* only managed to express viral mRNA to 6% of the total
 260 transcriptome, and the unmutated virion that infected *cell 105* still induced IFN. But in
 261 other cases, the stochasticity allows a defective virus to still escape immune recognition.
 262 For instance, there are a number of cells (e.g., *cell 62* and *cell 78*) that do not activate
 263 IFN despite being infected by virions that fail to express NS.

264 **Viral defects associated with infection outcome viral gene expression and
 265 IFN induction in single cells.** To systematically assess viral features associated with
 266 infection outcome, we divided the 150 cells in Fig. 4 into those that expressed unmu-
 267 tated copies of all eight genes (disregarding synonymous mutations) and those that did
 268 not. Fig. 5A shows that the 49 cells infected by full unmutated virions had a significantly
 269 tighter distribution of the amount of viral mRNA per cell than the other 101 cells as
 270 quantified by the Gini index (71). Therefore, viral defects are a major contributor to the
 271 heterogeneity in viral transcriptional burden.

272 Cells Some viral defects also contribute to IFN induction. Specifically, cells infected
 273 by incomplete or mutated virions also expressed IFN more frequently than cells in-
 274 fected by full wild-type virions virions that expressed unmutated copies of all genes
 275 (Fig. 5B), although this difference was not statistically significant ($P = 0.12$, Fisher's
 276 exact test). However, some specific viral defects were significantly associated with IFN

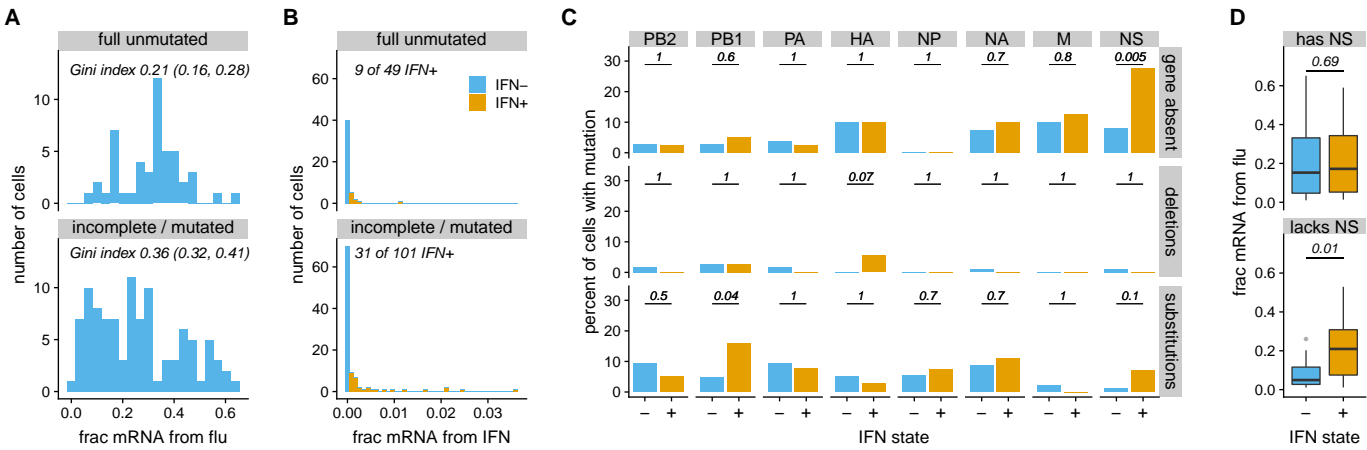


FIG 5 Viral features associated with heterogeneity in infection outcome among cells for which we determined viral genotypes. (A) Percent of all mRNA derived from virus, faceted by whether cells express unmutated copies of all eight genes. Cells infected by fully unmutated virions exhibit less heterogeneity in viral burden as quantified by the Gini index (95% confidence intervals are indicated). (B) IFN expression among cells expressing unmutated copies of all genes, and among cells with mutations or missing genes. (C) Specific viral defects associated with IFN induction. The top panel show the percent of IFN- and IFN+ cells that fail to express each viral gene. The middle and bottom panels show the percent of IFN- and IFN+ cells that have a deletion or amino-acid substitution in each gene, conditioned on the cell expressing that gene. Numbers give P-values (Fisher's exact test) for rejecting the null hypothesis that percents are equal among IFN- and IFN+ cells. (D) There is no association between IFN induction and the amount of viral mRNA in cells that express NS, but viral burden is associated with IFN induction among cells that lack NS. Throughout this figure, we only consider substitutions that are non-synonymous.

278 **induction** the association was significant for certain classes of viral defects: absence
 279 of NS and amino-acid mutations in PB1 were significantly enriched in IFN+ cells, and
 280 amino-acid mutations in NS and deletions in HA were weakly enriched (Fig. 5C). The
 281 only trend that remained significant at a false discovery rate (FDR) of 10% was absence
 282 of NS. This lack of statistical significance after FDR correction could be due to the
 283 relatively modest number of fully sequenced infected cells (just 150). The validation
 284 experiments in the next section show that many of the viral mutations in IFN+ cells do
 285 in fact increase the rate of IFN induction.

286 One other interesting trend emerges from the single-cell data. There is no difference
 287 in the amount of viral mRNA between IFN+ and IFN- cells that express NS (Fig. 5D).
 288 But among cells that lack NS, cells with more viral mRNA are significantly more likely
 289 to be IFN+ (Fig. 5D). **This**: this finding is elaborated on in the validation experiments
 290 below. Overall, the lack of reduced viral gene expression in IFN+ cells suggests that
 291 autocrine IFN signaling typically occurs too late to suppress viral transcription, and
 292 the well-known inhibitory effect of IFN against influenza depends mainly on paracrine
 293 signaling.

294 **Validation that viral defects in single IFN+ cells often increase IFN induction.**
 295 To test if the viral defects identified in single IFN+ cells cause increased IFN expression,
 296 we used reverse genetics to generate bulk stocks of viruses with some of these defects.

297 The viral defect most strongly associated with IFN induction was failure to express
 298 the NS gene (Fig. 4, Fig. 5C). Although it is sometimes possible to use complementing
 299 cells to generate influenza viruses lacking a specific gene (72, 73), we were unable to
 300 generate viruses that lacked NS. The NS gene encodes two proteins (NS1 and NS2), the
 301 first of which is influenza's primary innate-immune antagonist (24, 25). We therefore
 302 mimicked the absence of NS by creating a mutant virus (which we term "NS1stop") that
 303 had multiple stop codons early in the NS1 coding sequence.

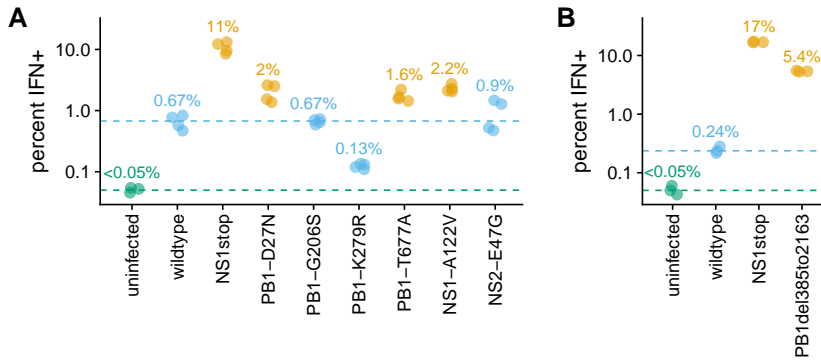


FIG 6 Validation that IFN induction is increased by some of the mutations identified in the single-cell virus sequencing of IFN+ cells. (A) Percent of infected cells that become IFN+ after infection with a bulk stock of the indicated viral mutant, as determined using a reporter cell line. The numbers indicate the median of four measurements for each viral mutant. The limit of detection of 0.05% is indicated with a dashed green line, and the median value for the wild type viral stock is indicated with a dashed blue line. Points are colored orange if the mutant virus stock induces IFN more frequently than the wild-type viral stock (one-sided t-test, $P < 0.01$), and blue otherwise. (B) Similar to the first panel, but validates increased IFN induction for a large internal deletion in the PB1 gene, and normalizes infecting virion dose rather than calling IFN+ percentage only among infected cells. See Fig. S12 and Fig. S13 for details. The experiments in the two panels were performed on different days, and so numerical values can be reliably compared within panels but not between panels.

304 The single-cell data also showed that amino-acid substitutions in proteins encoded
 305 by the PB1 and NS genes were enriched in IFN+ cells (Fig. 4, Fig. 5C), so we created
 306 mutant viruses with some of these substitutions: PB1-D27N, PB1-G206S, PB1-K279R,
 307 PB1-T677A, NS1-A122V, and NS2-E47G.

308 Finally, prior work has suggested that virions with internal deletions in the poly-
 309 merase genes can induce higher levels of IFN (16, 38, 39, 40, 41, 42). Although such
 310 deletions are not significantly enriched among IFN+ cells in our single-cell data (Fig. 5C),
 311 there is a co-infected IFN+ cell where one viral variant has a deletion in PB1 spanning
 312 nucleotides 385 to 2163 (cell 5 in Fig. 4). We therefore created a virus carrying this
 313 deletion, and propagated it in cells constitutively expressing PB1 protein.

314 We tested the rate of IFN induction by each viral stock using the reporter cells.
 315 Fig. 6 shows that five of the eight mutant viral stocks induced IFN more frequently than
 316 a wild-type viral stock. The strongest IFN induction was by the NS1stop virus, but the
 317 PB1 internal deletion and three of the point-mutant viruses (PB1-D27N, PB1-T677A,
 318 and NS1-A122V) also induced IFN significantly more frequently than wild type. The
 319 other three point mutants (PB1-G206S, PB1-K279R, and NS2-E47G) did not increase
 320 IFN induction—an unsurprising finding, since we expect some mutations without an
 321 IFN-enhancing effect to be found in IFN+ cells by chance. Overall, the results in Fig. 6
 322 validate that the viral defects in single IFN+ cells often cause increased IFN production.

323 However, IFN induction remains stochastic even for the most potently IFN-inducing
 324 viral mutants. Fig. 6 shows flow cytometry data (see also Fig. S12), which is itself a
 325 single-cell measurement, albeit one that does not report the viral genotype. As can
 326 be seen from these data, none of the mutant viral stocks induce IFN in more than
 327 20% of infected cells. Of course, these mutant virus stocks are themselves genetically
 328 heterogeneous, as many virions will have additional defects similar to that revealed by
 329 our single-cell sequencing of the “wild-type” viral stock. But our single-cell data show

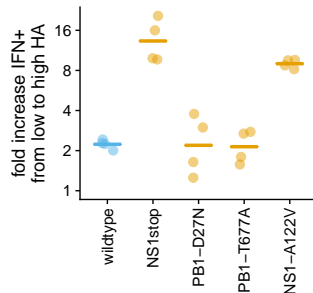


FIG 7 Infected cells that express higher levels of HA protein are much more likely to induce IFN expression only if they are infected by virus with defects in NS1. The y-axis shows the ratio of the percent of IFN+ cells in the highest HA-expression quartile relative to the lowest HA-expression quartile. Points indicate replicates, and lines indicate the mean. This figure is based on joint analysis of the IFN reporter and HA staining for all infected cells in the flow cytometry data in Fig. S12; see Fig. S14 for more details.

330 that IFN induction is stochastic even for infections that share the same defect, such as
 331 absence of NS (e.g., compare *cell 62* and *cell 69* in Fig. 4). Therefore, the experiments in
 332 this section not only validate some specific viral defects that increase IFN induction,
 333 but also show that induction remains stochastic even with these defects.

334 **The IFN-inducing viral defects act by diverse mechanisms.** Some of the viral
 335 defects in IFN+ cells are easy to reconcile with existing knowledge: for instance, NS1
 336 is the virus's primary IFN antagonist (24, 25), and internal deletions are prevalent
 337 in immunostimulatory viral stocks (16, 38, 39, 40, 41, 42). Other defects are more
 338 surprising: for instance, it is not obvious why amino-acid mutations in PB1 increase IFN
 339 induction. We therefore designed experiments to interrogate some of these defects in
 340 more detail.

341 We first focused on one of the strongest trends from the single cell data: increased
 342 viral gene expression is associated with increased IFN induction when the infecting
 343 virion fails to express NS, but not otherwise (Fig. 5D). To confirm this observation,
 344 we performed a flow cytometry analysis of the reporter cells infected by different
 345 immunostimulatory viral mutants to examine the association between expression of a
 346 viral gene product (HA protein) and IFN induction. Consistent with the single-cell data,
 347 cells that expressed more HA were much more likely to turn IFN+ when infected with
 348 the NS1stop or NS1-A122V mutants, but not when infected with any of the other viral
 349 variants (Fig. 7). This fact suggests that when there are high levels of viral transcription,
 350 NS1 becomes more important as a buffer against detection of viral products.

351 We hypothesized that the immunostimulatory mutations to PB1 might cause the
 352 viral polymerase to produce aberrant products, in line with recent work showing that
 353 mutations to PB2 can lead to the generation of aberrant RNAs that trigger RIG-I (35, 36).
 354 To investigate if the PB1 mutations might perturb polymerase activity, we examined
 355 their location in a structural model of the polymerase complex (Fig. 8A). The IFN-
 356 enhancing PB1 mutation T677A occurs at the tip of a helix that interacts with the 3'
 357 terminus of the RNA template as it enters the channel above the active site, whereas
 358 the IFN-enhancing D27N mutation is deeper in the polymerase close to the binding
 359 pocket of the 5' terminus of the template. Therefore, both mutations could plausibly
 360 alter the polymerase's interactions with the RNA template.

361 To test if the PB1 mutations affect activity, we transfected 293T cells with plasmids
 362 that express wild-type or mutant PB1 protein along with the other proteins in the
 363 polymerase complex (PB2, PA, and NP) and full-length viral RNA (vRNA) for the NA

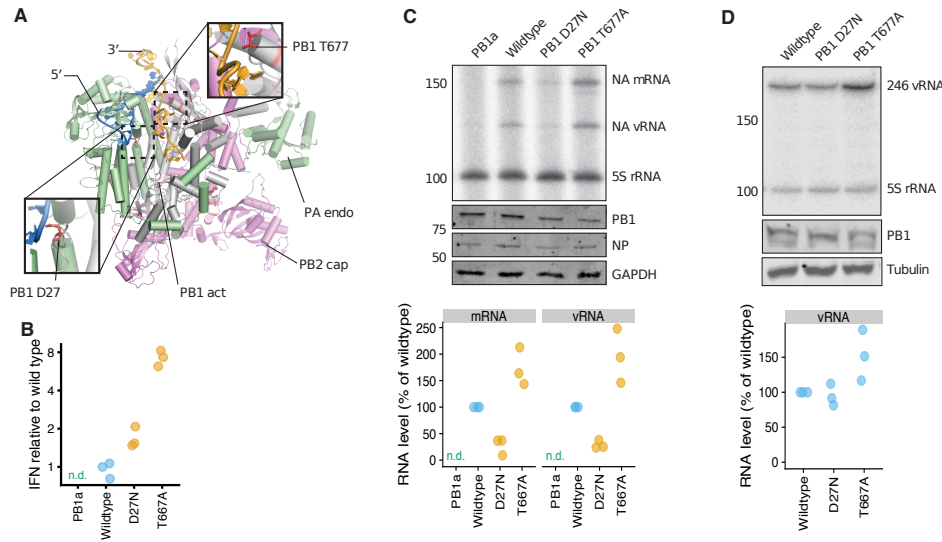


FIG 8 IFN-inducing mutations D27N and T677A in the PB1 protein affect polymerase activity. (A) Model of bat influenza A virus polymerase (PDB 4WSB) (74) superposed with the influenza B virus polymerase (PDB 5MSG) (75). The locations of PB1 D27 and T677 (both red) relative to the 5' (blue) and 3' (orange) termini of the RNA template and the PB1 active site (grey; PB1 act) are indicated. The PA endonuclease (green; PA endo) and PB2 cap binding domain (pink; PB2 cap) are also indicated. Part of the fingers subdomain of PB1 is hidden to reveal the template in the entry channel. (B) IFN-beta promoter activity measured using a dual luciferase reporter assay in 293T cells transfected with plasmids expressing the indicated PB1 protein, the other polymerase complex proteins (PB2, PA, and NP), and a full-length NA vRNA template. PB1a is a catalytically inactive PB1 active site control. In this panel and the next two panels, points show three biological replicates; “n.d.” indicates not detectable, and orange indicates a variant was significantly different than wild type by a two-sided t-test. (C) Polymerase activity on full-length vRNA template in 293T cells transfected as in panel (B). Steady-state RNA levels were measured by primer extension, denaturing PAGE, and phosphorimaging. PB1a was used as negative control and background correction. The 5S rRNA signal was used as loading control. Other panels show Western blot analysis of PB1, NP and GAPDH protein expression, and the graph at the bottom shows quantification by phosphorimaging. (D) Polymerase activity on a short 246-nucleotide vRNA template. The top panel shows the steady state levels of vRNA template as determined by primer extension and denaturing PAGE. The other two panels show the PB1 and tubulin expression levels analyzed by Western blot, and the graph shows quantification.

364 segment. Both polymerase mutations increased IFN expression in this assay (Fig. 8B),
 365 indicating that they have an immunostimulatory effect in the context of an active
 366 viral polymerase even when other viral components are absent. We next directly
 367 measured polymerase activity on the full-length vRNA template by extracting total
 368 RNA and quantifying replication (vRNA) and transcription (mRNA) products by primer
 369 extension. Both immunostimulatory PB1 mutations had activities that were significantly
 370 different from wild type, despite being expressed at wild-type protein levels (Fig. 8B).
 371 Specifically, T677A had higher levels of both activities, whereas D27N had reduced
 372 levels of both—although D27N still retained activity far in excess of a control active-site
 373 mutant (Fig. 8C). We speculated that the mutations might alter polymerase processivity,
 374 leading to accumulation of aberrant RNA products that activate the innate immune
 375 system (35, 38, 39, 40, 41, 42). We therefore repeated the activity assays using a
 376 short 246-nucleotide template (35) in place of the full-length NA vRNA (Fig. 8D). On
 377 this shorter template, the activity of the D27N mutant was now similar to wild type,
 378 while the activity of the T677A mutant remained higher than wildtype (although not

379 significantly so in three biological repeats). Therefore, the two immunostimulatory PB1
 380 mutations have distinct effects on the polymerase: D27N reduces processivity thereby
 381 favoring shorter RNA products, whereas T677A increases overall activity which could
 382 also lead to accumulation of aberrant RNA products.

383 Overall, the results in this section show that the diverse range immunostimulatory
 384 viral defects identified in single cells act by diverse processes, showing that viral varia-
 385 tion influences not only the rate of IFN induction but also the factors that contribute to
 386 this induction.

387 DISCUSSION

388 We have determined the full sequences of all viral genes in single influenza-infected
 389 cells. Methodologically, our major advance is to measure the *genotypes* of viruses in
 390 addition to the abundance of viral components (i.e., transcripts, proteins, or progeny
 391 virions) as has been done by prior single-cell studies (12, 13, 15, 16, 14, 43, 45, 46,
 392 47, 48, 76, 77, 78). Our method builds on the observation that fragmentary viral
 393 genetic information can be obtained by more standard single-cell transcriptomic tech-
 394 niques (16, 46, 47). To make this information complete, we have coupled single-cell
 395 transcriptomics with long-read PacBio sequencing of viral genes, a strategy analogous
 396 to that used by (79) to obtain full-length isoforms of some cellular genes in single cells.

397 This viral genetic information is crucial for understanding infection outcome helps
 398 explain cell-to-cell variation in viral gene expression and innate-immune induction.
 399 Despite the fact that we used a low-passage viral stock generated from plasmids, most
 400 infected cells do not express unmutated copies of all viral genes. Although our study is
 401 certainly not the first to note that influenza has a high mutation rate (30, 31, 32, 33, 34)
 402 and sometimes fails to express genes (12, 15, 43, 60, 61), it is the first to directly observe
 403 the full spectrum of these defects across single cells. Visual inspection of Fig. 4 shows
 404 how any experiment that does not sequence viral genes in single cells is averaging
 405 across a diverse spectrum of viral defects.

406 We identified four types of defects that we validated to increase IFN induction.
 407 Two types of defects—absence of the NS gene and amino-acid mutations to the
 408 NS1 protein—presumably impair NS1's well-known ability to antagonize innate im-
 409 munity (24, 25). But although the general role of NS in innate-immune antagonism
 410 has long been appreciated, our work represents the first direct demonstration that
 411 stochastic absence and mutations to this gene are a major contributor to IFN induction
 412 in single cells. A third type of defect, amino-acid mutations in PB1, was more surpris-
 413 ing since this protein has not been described as a major player in innate-immune
 414 detection. We characterized two IFN-inducing PB1 mutations, and showed that one
 415 impaired polymerase processivity whereas the other increased overall activity. We
 416 speculate that these alterations increase production of aberrant immunostimulatory
 417 RNA products (35). Finally, we found an internal deletion in PB1 that enhances IFN
 418 induction, consistent with prior work showing such deletions are immunostimula-
 419 tory (38, 39, 40, 41, 42). In fact, given the extensive prior work on deletions, we were
 420 surprised not to identify more of them in our IFN+ cells. There may be several reasons:
 421 we used pure viral stocks (53) at modest MOI; our experiments preferentially captured
 422 cells with higher viral transcriptional load; and most prior studies have used techniques
 423 that can detect large deletions but not subtle point mutations. Additionally, the relative
 424 importance of different defects likely varies across infection conditions, viral strains,
 425 and cell types: it is an open question which defects are most relevant for immune
 426 detection during actual human infections.

427 However, the greatest value of our work is not as a screen for IFN-inducing defects,

428 but rather as a relatively unbiased survey of the breadth of viral variation in individual
 429 infected cells. This survey shows that no single type of viral defect determines whether
 430 a cell induces IFN: even the most immunostimulatory defect (absence of NS) occurs in
 431 only about a quarter of IFN+ cells. Therefore, innate-immune detection of influenza is
 432 a multi-faceted process that cannot be ascribed a single dominant viral genetic cause.

433 Our results further show that viral genetic defects ~~only partially do not fully~~ explain
 434 the heterogeneity among influenza-infected cells. There is substantial breadth in viral
 435 transcriptional burden and occasional IFN induction even among cells infected with
 436 unmutated virions. Additionally, no viral defect induces IFN deterministically: every type
 437 of immunostimulatory defect that we characterize is also observed in IFN- cells in our
 438 single-cell dataset. ~~This fact shows that Therefore~~, stochasticity or pre-existing cellular
 439 states ~~also~~ play a major role in affecting ~~the outcome of infection—a innate-immune~~
 440 ~~induction—a~~ finding that concords with the fact that IFN induction is heterogeneous
 441 even among cells treated with synthetic innate-immune ligands (20, 21, 22, 23), as well
 442 as for other viruses (48).

443 Perhaps the most intriguing question is how the heterogeneity that we have
 444 described ultimately affects the macroscopic outcome of infection. Natural human
 445 influenza infections are established by just a handful of virions (17, 18, 19) that then
 446 undergo exponential growth, and early IFN responses are amplified by paracrine sig-
 447 naling (1, 2). It is therefore plausible that early heterogeneity ~~could affect downstream~~
 448 ~~events in innate-immune induction could affect the entire course of infection~~. Extend-
 449 ing our approaches to more complex systems could shed further light on how viral
 450 genetic variation ~~interacts with cell-to-cell heterogeneity and stochasticity interact~~ to
 451 shape the race between virus and immune system.

452 MATERIALS AND METHODS

453 **IFN reporter cell lines.** We created IFN reporter variants of the A549 human lung epithelial
 454 cell line (Fig. 1A). The parental A549 cell line used to create these reporters was obtained
 455 from ATCC (CCL-185), and was tested as negative for mycoplasma contamination by the Fred
 456 Hutch Genomics Core and authenticated using the ATCC STR profiling service. The cells were
 457 maintained in D10 media (DMEM supplemented with 10% heat-inactivated fetal bovine serum,
 458 2 mM L-glutamine, 100 U of penicillin / ml, and 100 µg of streptomycin / ml) at 37°C and 5%
 459 carbon dioxide.

460 To create the type I interferon reporters, a 1kb promoter region upstream of the human
 461 IFNB1 gene were cloned into the pHAGE2 lentiviral vector (80), with a NotI site immediately
 462 downstream of the promoter serving as an artificial Kozak sequence. Downstream of this
 463 NotI site, each of the following reporter constructs was cloned: mCherry, mNeonGreen, and
 464 low-affinity nerve growth factor lacking the C-terminal signaling domain (LNGFRΔC) (49, 50)
 465 linked to mNeonGreen by a P2A linker (81). The sequence of the last of these constructs is
 466 provided in File S1.

467 To create the type III interferon reporters, a 1.2kb region upstream of the human IL29
 468 (IFNL1) gene was cloned into the pHAGE2 vector, with the native Kozak sequence retained at
 469 the 3' end. Downstream of this promoter we cloned LNGFRΔC linked to ZsGreen via a P2A
 470 linker. The sequence of this construct is provided in File S1.

471 We used these constructs to generate lentiviral vectors and transduce of A549 cells in the
 472 presence of 5 µg polybrene. We then sorted single transduced cells and expanded them. A
 473 portion of the expanded cells were tested for reporter activity by transfecting poly(I:C) (a potent
 474 agonist of the RIG-I pathway), and we retained clones with strong activation. Importantly, the
 475 cells that we retained for further use were not the same portion that were tested by poly(I:C)
 476 treatment, but rather a separate split of the same population—this avoids any selection on the
 477 cells from transient activation of IFN. For the dual type I / type III reporter used in Fig. S1B, a
 478 single-cell clone of the type III reporter cell line was transduced with the type I reporter bearing
 479 the mCherry fluorescent marker, and then isolated and propagated as a single cell clone for

480 the other cell lines. All reporter lines tested negative for mycoplasma contamination by the
 481 Fred Hutch Genomics Core.

482 Fig. S1A shows validation of the reporter cell lines using infection with saturating amounts
 483 of the Cantell strain of Sendai virus (obtained from Charles River Laboratories). For detection
 484 of the cell-surface bound LNGFR Δ C, cells were stained with PE-conjugated anti-LNGFR (CD271)
 485 antibody from Miltenyi Biotec.

486 **Viruses for single-cell experiments.** We performed the single-cell experiments using the
 487 A/WSN/1933 (H1N1) strain of influenza virus. We used both the wild-type virus and a variant
 488 of the virus where synonymous mutations were added within a few 100 nucleotides of each
 489 termini of each gene segment. We have used a similar synonymous viral barcoding strategy in
 490 our prior single-cell work (12) as it allows us to detect about half of co-infected cells based on
 491 the expression of both viral barcode variants. In the current work, we extended this approach
 492 by placing synonymous barcodes near *both* termini of the gene segments in order to quantify
 493 strand exchange during PacBio sequencing (Fig. S10). The sequences of all gene segments from
 494 the wild-type and synonymously barcoded viral strains are in File S2. These genes were cloned
 495 into the pHW2000 (52) reverse-genetics plasmid.

496 Both viral strains were generated by reverse genetics using the pHW18* series of bi-
 497 directional plasmids (52). We controlled the durations and MOI during viral passaging since
 498 these factors can greatly affect the accumulation of defective viral particles (53). The viruses
 499 were generated by reverse genetics in co-cultures of 293T and MDCK-SIAT1 cells in influenza
 500 growth media (Opti-MEM supplemented with 0.01% heat-inactivated FBS, 0.3% BSA, 100 U
 501 of penicillin/ml, 100 μ g of streptomycin/ml, and 100 μ g of calcium chloride/ml) and then
 502 propagated in MDCK-SIAT1 cells in influenza growth media using the same basic procedures
 503 detailed in (12). Specifically, after generation by reverse genetics, the wild-type variant was
 504 expanded at an MOI of 0.001 for 72 hours twice in MDCK-SIAT1 cells, and the synonymously
 505 barcoded variant was expanded once at an MOI of 0.01 for 60 hours. The MOIs for this
 506 passaging are based on titers determined using TCID50 assays via the formula of Reed and
 507 Muench (82) as implemented at <https://github.com/jbloomlab/reedmuenchcalculator>. After
 508 being passaged independently, the two viral stocks were combined at equivalent numbers of
 509 infectious units to make the stock used in the single-cell experiments.

510 **Flow cytometry analyses for HA expression.** For the single-cell experiments (which only
 511 examine the transcriptional results of a single cycle of infection), we were most interested in
 512 the titer of viral particles that are transcriptionally active for a single round of infection of A549
 513 cells. We estimated titers of transcriptionally active virions by staining for HA expression in
 514 virus-infected A549 cells. Specifically, we infected A549 cells (or one of the A549 reporter cell
 515 line variants as indicated) in influenza growth medium, and at 13 to 14 hours post-infection,
 516 we trypsinized cells, re-suspended in phosphate-buffered saline (PBS) supplemented with 2%
 517 heat-inactivated fetal bovine serum (FBS), and stained with 10 μ g/ml of H17-L19, a mouse
 518 monoclonal antibody previously shown to bind to the HA from the A/WSN/1933 strain of
 519 virus (83). After washing in PBS supplemented with 2% FBS, the cells were stained with a goat
 520 anti-mouse IgG antibody conjugated to APC, washed, fixed in 1% formaldehyde in PBS, washed
 521 again, and then analyzed by flow cytometry to determine the fraction expressing detectable HA
 522 protein.

523 **Single-cell transcriptomics of IFN-enriched infected cells using 10X Chromium.** The
 524 single-cell transcriptomics and virus sequencing was performed using the A549 cells with the
 525 *IFNB1* LNGFR Δ C-P2A-mNeonGreen reporter. A schematic of the experiment is shown in Fig. 2.

526 The wild-type and synonymously barcoded viruses were mixed with the goal of adding
 527 equal numbers of transcriptionally active HA-expressing virions of each virus strain. The cells
 528 were then infected with this mixture at a dose designed to infect about half the cells (Fig. 3C
 529 suggests that the actual rate of detectable infection was slightly lower). Infections were allowed
 530 to proceed for 12 hours. The cells were then trypsinized, the trypsin was quenched with D10
 531 media, and cells were resuspended in de-gassed PBS supplemented with 0.5% bovine serum
 532 albumin and 5 mM EDTA. To enrich IFN+ cells, the cells were then incubated with anti-LNGFR
 533 MACSelect Microbeads (Miltenyi Biotec) and twice passed over an MS magnetic column (Miltenyi
 534 Biotec), retaining the bound (and presumably IFN-enriched) population each time. This MACS
 535 sorting is expected to give approximately the enrichment for IFN+ cells shown in Fig. S3. The

536 original, unsorted, population was then added back in to ~10% of the final cell fraction in
 537 order to ensure the presence of interferon negative cells. At this point, uninfected canine
 538 (MDCK-SIAT1) cells were also added to ~5% of the final cell fraction to enable quantification
 539 of the cell multiplet rate ([Fig. 3A](#)) and background viral mRNA in uninfected cells ([Fig. 3C](#)). We
 540 began this entire process of cell collection and enrichment at 12 hours post-infection, but
 541 the process (which was performed at room temperature) took about an hour, and thus we
 542 consider the cells to have been analyzed at 13 hours post-infection. The final cell suspension
 543 was counted using a disposable hemocytometer and loaded on the 10x Genomics Chromium
 544 instrument ([54](#)), targeting capture of ~1,500 cells.

545 This sample was then processed to create libraries for Illumina 3'-end sequencing according
 546 to the 10X Genomics protocol using the Chromium Single Cell 3' Library and Gel Bead Kit v2
 547 with one important modification: rather than process all full-length cDNA through enzymatic
 548 fragmentation, several nanograms were retained for targeted full-length viral cDNA sequencing
 549 as described below. The single-cell transcriptomics library was sequenced on an Illumina HiSeq
 550 2500, and the data analyzed as described below.

551 **Enrichment and preparation of viral cDNA for PacBio sequencing.** We amplified virus-
 552 derived molecules from cDNA retained from the 10X Genomics protocol for PacBio sequencing
 553 of the full-length cDNA. These cDNA have at their 3' end the cell barcode and UMI plus the
 554 adaptor sequence that is added during the 10X protocol (see [Fig. 2](#) for simple schematic, and
 555 [File S7](#) for more details). We only wanted to PacBio sequence cDNA molecules derived from
 556 virus. We therefore needed to enrich for the viral molecules while retaining the 10X adaptor /
 557 UMI / cell barcode at the 3' end.

558 We first performed a multiplex PCR reaction on 1 ng of the full-length 10X cDNA using a 3'
 559 primer complementary to the common 10X adaptor, and a multiplex mix of eight 5' primers,
 560 one specific for the mRNAs from each of the eight viral gene segments ([File S3](#)). A major
 561 concern during these PCRs is strand exchange (see [Fig. S10](#)) which would scramble the cell
 562 barcodes and mutations on viral cDNAs. To reduce strand-exchange and obtain more even
 563 PCR amplification across segments, we performed emulsion PCRs using the Micellula DNA
 564 Emulsion Kit (Roboklon), which physically separates disparate template molecules, preventing
 565 strand exchange and allowing each molecule to be amplified to exhaustion of its droplet's
 566 reagents ([84](#)). We performed the PCRs using Kapa HiFi Hotstart ReadyMix, supplementing the
 567 reactions with additional BSA to a final concentration of 0.1 mg/ml and using a volume of 100 μ l.
 568 Both the common 3' primer and the multiplex mix of eight 5' primers were added to a final
 569 concentration of 0.5 μ M. We performed 30 cycles of PCR, using an extension time of 2 minutes
 570 15 seconds at 67°C, and a melting temperature of 95°C. This melting temperature is lower
 571 than the standard 98°C melting step suggested by the manufacturer for Kapa HiFi because we
 572 wanted to avoid collapse of emulsion integrity at high temperature.

573 The product of this multiplex PCR was subjected to eight additional individual emulsion
 574 PCR reactions, each using only a single segment-specific 5' primer as well as the common 3'
 575 primer, using 1 ng of material in each reaction. The material from these eight segment-specific
 576 PCRs was then pooled with the goal of obtaining an equimolar ratio of segments, and sequenced
 577 on one SMRT Cell in a PacBio RS II and one SMRT Cell of a PacBio Sequel. Detailed results from
 578 the analysis of these first two sequencing runs is shown in [File S7](#). These results showed that
 579 although the PCRs substantially enriched for influenza molecules, the relative coverage of the
 580 different viral genes was still uneven, with the longer genes under-sampled.

581 To improve coverage of the polymerase genes, we produced two new sequencing pools:
 582 one consisting of the five shortest viral segments (HA, NP, NA, M, and NS) from the afore-
 583 mentioned segment-specific emulsion PCRs, and the other consisting of the three longer
 584 polymerase segments (PB2, PB1, and PA). The former was sequenced on one cell of a single
 585 SMRT Cell of a PacBio Sequel, and the latter on two additional SMRT Cells of a PacBio Sequel.
 586 As is shown [File S7](#), the coverage remained relatively low for the polymerase genes—and
 587 most of the reads we did obtain were dominated by shorter internally deleted variants of the
 588 polymerase genes ([53](#)) which are preferentially amplified during PCR.

589 To obtain more reads for longer full-length polymerase variants, we therefore subjected 10
 590 ng of our amplified material for each polymerase segment to a bead selection using SPRIselect
 591 beads at a volume ratio of 0.4. This selection removes most low-molecular weight DNA species

592 including internally-deleted defective segments. Material from this selection was amplified
 593 using 16 (PB1) or 14 (PB2 and PA) cycles of a non-emulsion PCR using the standard conditions
 594 recommended by the Kapa HiFi Hotstart ReadyMix (extension at 67°C for 2 minutes 15 seconds,
 595 and melting at 98°C). The use of relatively few PCR cycles was designed to prevent the
 596 occurrence of the artifacts (including strand exchange) that occur in non-emulsion PCRs. We
 597 pooled the products of these reactions from this size-selection and sequenced on a SMRT Cell
 598 of a PacBio Sequel. As is shown in [File S7](#), this sequencing yielded more full-length polymerase
 599 variants, but they were still undersampled compared to other viral genes.

600 To further to improve recovery of full-length PB1, PB2, and PA, we use an approach that
 601 allowed us to perform a specific PCR for full-length polymerase variants. We circularized the
 602 template molecules, and then used two segment-specific primers that annealed in apposition
 603 near the center of each polymerase gene to linearize these circular molecules. Only molecules
 604 that contain the middle of the polymerase genes (which are typically full-length) are linearized
 605 by this process. In the downstream computational analysis, we can then determine the full
 606 sequence of the gene as well as the cell barcode of the initial molecule from which the linearized
 607 molecule is derived. Specifically, we first used 2.5 ng of our already-amplified segment-specific
 608 material in a 10-cycle PCR to append circularization adapters (see [File S3](#) for sequences), and
 609 cleaned the resultant mixture using SPRIselect beads at a volume ratio of 0.4. We then used 10
 610 ng of this amplified material in a 20µl NEBuilder reaction using an extended reaction time of 50
 611 minutes in order to circularize the molecules. We next incubated these reactions for 1 hour
 612 at 37°C with exonuclease V and additional ATP to a final increase in concentration of 1 mM to
 613 digest all non-circularized molecules. The circularized and digested material was then cleaned
 614 using SPRIselect beads at a volume ratio of 0.4. This material was then used as template for
 615 three non-emulsion PCRs specific to PB2, PB1, or PA, using two segment-specific primers that
 616 align to the central portion of each gene but in apposition to each another (see [File S3](#) for
 617 sequences). These linearization reactions used 20 (PB2) or 26 (PB1 and PA) PCR cycles, and the
 618 resulting products were cleaned using SPRIselect beads at a volume ratio of 1.0. This material
 619 was pooled to produce an equimolar mixture of full-length PB1, PA, and PB2 and sequenced
 620 in an additional SMRT Cell of PacBio Sequel. As is shown in [File S7](#), this process yielded many
 621 full-length polymerase variants.

622 The computational analyses of the full-length viral gene sequences described below com-
 623 bined the data from all these reactions. The number of sequences obtained for each gene after
 624 pooling the data from all reactions is shown in [Fig. S9](#), which also indicates that the net rate
 625 of strand exchange is very low (see [Fig. S10](#) for an illustration of how this is determined). A
 626 detailed breakdown of the coverage of each gene and PacBio run is in [File S7](#). Importantly, the
 627 PCR biases mean that the coverage of molecules by the PacBio sequencing is not proportional
 628 to their abundance in the starting mRNA. However, as described in the computational anal-
 629 ysis section below, the final analyses use the cell barcodes and UMLs in conjunction with the
 630 standard 10X Illumina sequencing to ensure that none of the conclusions are affected by the
 631 disproportionate amplification of some molecules during the PacBio library preparation (for
 632 instance, duplicate UMLs are removed from the PacBio data, and all conclusions about gene
 633 abundance or absence are based on the Illumina data).

634 **qPCR for viral genes and IFN.** We performed qPCR on reverse-transcribed mRNA for
 635 influenza HA (to quantify viral transcription), IFNB1 (to quantify IFN induction), and L32 (a
 636 cellular housekeeping gene for normalization). For the qPCR, we used the SYBR Green
 637 PCR Master Mix (Thermo Fisher) according to the manufacturer's protocol using oligo-dT
 638 primers. The qPCR primers were: HA primer 1, 5'-GGCCCAACCACACATTCAAC-3'; HA primer
 639 2, 5'-GCTCATCACTGCTAGACGGG-3'; IFNB1 primer 1, 5'-AAACTCATGAGCAGTCTGCA-3'; IFNB1
 640 primer 2, 5'-AGGAGATCTCAGTTGGAGG-3'; L32 primer 1, 5'-AGCTCCAAAATAGACGCAC-3';
 641 L32 primer 2, 5'-TTCATAGCAGTAGGCACAAAGGG-3'.

642 For the qPCR in [Fig. S13](#), A549 cells were seeded at a density of 10^4 cells/well in a 96-
 643 well plate in D10 media 24 hours prior to infection, with four independent wells seeded per
 644 experimental treatment. Immediately prior to infection D10 media was removed and replaced
 645 with influenza growth media and infected with the indicated influenza strains at a MOI of
 646 0.4 based on TCID50 in MDCK-SIAT1 cells. For the cells with cycloheximide added to block
 647 protein expression (and hence secondary transcription), cycloheximide was added to a final

concentration of 50 µg/ml (a concentration sufficient to block secondary transcription (85)) at the time of infection. After 8 hours, mRNA was harvested using the CellAmp Direct RNA Prep Kit for RT-PCR, reverse-transcribed using an oligo-dT primer, and qPCR was performed as described above.

Viruses and experiments for validation experiments. In Fig. 6, we tested the IFN inducing capacity of a variety of viral mutants identified in the single-cell experiments. For point-mutant viruses, we created variants for all amino-acid substitutions found in PB1 and NS among IFN+ cells that did not also lack NS. One of these mutants (amino-acid substitution S704P in PB1) did not reach sufficient titers in a single attempt to generate it by reverse genetics, and so was dropped from the experiment (note that we did not attempt replicates of the reverse genetics for this mutant, and so are *not* confident in drawing strong conclusions about its actual attenuation). This left six point-mutant viruses: four with point mutations in PB1, and two with point mutations in NS. We also created a mutant virus that contained the internal deletion in PB1 found in an IFN+ cell. In addition, we created a virus with an inactivated NS1 to mimic the infections that failed to express NS (we were unable to use complementing cells to generate a viral stock that completely lacked the NS segment). This NS1stop virus contained six nucleotide changes resulting in the addition of five in-frame stop codons in NS1 starting 10 nucleotides downstream of the 5' splice donor site, thereby disrupting NS1 while leaving NS2 (NEP) intact. All of these mutants were cloned into the pHW2000 bi-directional reverse-genetics plasmid (52) in order to enable generation of viruses encoding the mutant genes. [File S6](#) provides the full sequences for all of these plasmids.

We generated the wild-type and point-mutant viruses for the validation experiments in Fig. 6A by reverse genetics using the pHW18* series of WSN reverse genetics plasmids (52), but substituting the appropriate mutant plasmid listed in [File S6](#) for the wild-type plasmid for that gene. To generate the viruses from these plasmids, we transfected an equimolar mix of all eight plasmids into co-cultures of 293T and MDCK-SIAT1 cells seeded at a ratio of 8:1. At 24 hours post-transfection, we changed media from D10 to influenza growth media. At 50 hours post-transfection (for the replicate 1 viruses in Fig. S12A) or 72 hours (for the replicate 2 viruses in Fig. S12), we harvested the virus-containing supernatant, clarified this supernatant by centrifugation at 300×g for 4 min, and stored aliquots of the clarified viral supernatant at -80°C. We then thawed aliquots and titered by TCID50 on MDCK-SIAT1 cells. For the infections in Fig. S12A, we wanted to use equivalent particle counts, so we normalized all viruses to an equivalent hemagglutination titer on turkey red blood cells (86). Briefly, a solution of 10% v/v red blood cells (LAMPIRE Biological Laboratories, Fisher Scientific catalogue number 50412942) was washed in PBS and diluted to a final concentration of 0.5% v/v. Two-fold serial dilutions of virus were added to an equal volume of diluted red blood cells, and titer was measured as the highest dilution of viral stock at which complete hemagglutination of red blood cells was observed. We then performed infections of the A549 reporter cell line at equivalent hemagglutination titer and analyzed the data as described in Fig. S12A.

To generate the NS1stop mutant virus and the wild-type and PB1del385to2163 mutant viruses in Fig. S12B, we used slightly different procedures. The wild-type virus was generated by reverse genetics as described for the point-mutant viruses above, harvested at 48 hours post-transfection, and then passaged on MDCK-SIAT1 cells for 36 hours at an MOI of 0.05—conditions that we previously validated to lead to relatively little accumulation of defective particles (12). The NS1stop virus was similarly generated, but was passaged for 48 rather than 36 hours, since it had slower growth kinetics and so needed a longer period of time to reach high titers. The viruses with deletions in the PB1 segment could not be generated in normal 293T and MDCK-SIAT1 cells, since they required the exogenous expression of the PB1 protein. Therefore, these viruses were generated in previously described 293T and MDCK-SIAT1 cells that had been engineered to constitutively express PB1 (87). These viruses were harvested from transfections at 72 hours, and passaged twice in the MDCK-SIAT1 cells constitutively expressing PB1 at a MOI of 0.001 for 72 hours and 0.01 for 48 hours. This passaging was necessary as viral titers from transfections were too low to generate sufficient virus from a single passage. The wild-type and NS1stop viruses were titered by TCID50 on MDCK-SIAT1 cells, and the PB1 deletion viruses were titered on the MDCK-SIAT1 cells constitutively expressing PB1. The infections in Fig. S12B were performed at equivalent TCID50s as described in the

704 legend to that figure. That these equivalent TCID50s were also roughly equivalent in terms of
 705 particles capable of undergoing primary transcription is shown in [Fig. S13](#).

706 **Computational analysis of single-cell transcriptomic and viral sequence data.** A com-
 707 putational pipeline that performs all steps in the data analysis is available at https://github.com/jbloomlab/IFNsorted_flu_single_cell. This pipeline is orchestrated by Snakemake (88), and
 708 begins with the raw sequencing data and ends by generating the figures shown in this paper.
 709 The sequencing data and annotated cell-gene matrix are available on the GEO repository under
 710 accession GSE120839 (<https://www.ncbi.nlm.nih.gov/geo/query/acc.cgi?acc=GSE120839>).

711 Briefly, the raw deep sequencing data from the Illumina 3'-end sequencing were processed
 712 using the 10X Genomics software package cellranger (version 2.2.0). We built a multi-species
 713 alignment reference consisting of a concatenation of the human and influenza virus transcrip-
 714 tomes (the first “species”) and the canine transcriptome (the second “species”). The human
 715 transcriptome was generated by filtering genome assembly GRCh38 for protein-coding genes
 716 defined in GTF file GRCh38.87. The influenza virus transcriptome consisted of the mRNAs for
 717 the wild-type A/WSN/1933 virus strain in [File S2](#) (the cellranger alignment is sufficiently permiss-
 718 ive that it aligns sequences from both the wild-type and synonymously barcoded viral variants
 719 to this transcriptome). The canine transcriptome was generated by filtering genome assembly
 720 CanFam3.1 for protein-coding genes defined in GTF file CanFam3.1.87. The cellranger software
 721 was used to align the Illumina 3'-end sequencing reads to this multi-species transcriptome, call
 722 human+influenza and canine cells ([Fig. 3A](#)), and generate a matrix giving the expression of each
 723 gene in each single cell. We used a custom Python script to determine the number of influenza
 724 virus reads that could be assigned to the wild-type or synonymously barcoded virus, and added
 725 this information to the annotated the cell-gene matrix.

726 The PacBio sequences of the full-length viral genes were analyzed as follows. First, we
 727 used version 3.1.0 of PacBio’s ccs program (<https://github.com/PacificBiosciences/unanimity>) to
 728 build circular consensus sequences (CCSs) from the subreads files, requiring at least 3 passes
 729 and a minimum accuracy of 0.999. We further processed these CCSs using custom Python
 730 code and the minimap2 (89) long-read aligner (version 2.11-r797). The Python code has been
 731 implemented in the API of dms_tools2 (https://jbloomlab.github.io/dms_tools2/ (90)) package
 732 (version 2.3.0). A Jupyter notebook that performs these analyses is at https://github.com/jbloomlab/IFNsorted_flu_single_cell/blob/master/pacbio_analysis.ipynb, and is also provided
 733 in HTML form as [File S7](#). We refer the reader to this notebook for a detailed description and
 734 extensive plots showing the results at each step. Here is a brief summary: we filtered for
 735 CCSs that had the expected 5' termini (from the influenza-specific primers) and 3' termini
 736 (corresponding to the 10X adaptor), and for which we could identify the cell barcode, UMI, and
 737 polyA tail. We aligned the cDNAs flanked by these termini to the influenza transcriptome, and
 738 performed a variety of quality control steps. At this point, we examined whether cDNAs had
 739 the synonymous viral barcodes at both ends or neither end as expected in the absence of
 740 strand exchange ([Fig. S10](#)), and reassuringly found that strand exchange was rare ([Fig. S9](#)). The
 741 small number of CCSs with identifiable strand exchange were filtered from further analysis. We
 742 then further filtered for CCSs that contained valid cell barcodes as identified by the cellranger
 743 pipeline, and kept just one CCS per UMI (preferentially retaining high-quality CCSs that aligned
 744 to full-length cDNAs). We then removed from the CCSs the barcoding synonymous mutations
 745 that we had engineered into one of the two viral variants. Finally, we used the CCSs to
 746 call the sequence of the viral gene in each cell, calling mutations separately for each viral
 747 barcode variant. We called mutations (insertions, deletions, and substitutions) in the viral gene
 748 sequences as follows:

- 751 1. Mutations with accuracies less than 0.999 (which constitute <0.5% of all mutations)
 752 were ignored.
- 753 2. If all CCSs for a particular viral-barcode variant of a gene in a cell were wild-type, it was
 754 called as wild type.
- 755 3. If any CCSs for a particular viral-barcode variant of gene in a cell had a mutation, then
 756 require at least two CCSs to call the sequence.
- 757 4. If at least two and >30% of the CCSs had a specific mutation, then call that mutation as
 758 present and note its frequency among the CCSs. The exception was single-nucleotide
 759 indels in homopolymers, for which we required three CCSs to call a mutation (the reason

760 is that the main mode of PacBio sequencing errors is short indels in homopolymers).
 761 The plots in [File S7](#) indicate that these are reasonable mutation-calling criteria. We could call
 762 the sequences of all expressed viral genes in about half of the infected cells ([Fig. S11](#)). The
 763 mutations called using this pipeline are shown in [Fig. 4](#), and [File S4](#) gives the number of CCSs
 764 supporting each mutation call. The called sequences of the viral genes were added to the
 765 annotated cell-gene matrix.

766 Finally, we process the annotated cell-gene matrix in R to generate the plots shown in
 767 this paper. This analysis utilized a variety of R and Bioconductor (91) packages, including
 768 Monocle (92, 93) and ggplot2. A Jupyter notebook that performs these analyses is at https://github.com/jbloomlab/IFNsorted_flu_single_cell/blob/master/monocle_analysis.ipynb, and
 769 is also provided in HTML form as [File S8](#). We refer the reader to this notebook for a detailed
 770 description and a variety of additional plots not included in the paper. Briefly, we first filtered
 771 cells that were extreme outliers in the amount of mRNA as shown in [Fig. 3B](#). We used the
 772 uninfected canine cells to estimate the percentage of total mRNA in a cell that would come
 773 from influenza purely due to background (e.g., from cell lysis) in the absence of infection, and
 774 called as infected the human cells for which significantly more than this amount of mRNA
 775 was derived from influenza under a Poisson model ([Fig. 3C](#)). We next used a Poisson model
 776 parameterized by the amount of expected background mRNA for each influenza gene to call
 777 the presence or absence of each influenza gene in each infected cell ([Fig. 3D](#) and [Fig. S4](#)). To
 778 identify cells that were co-infected with both viral barcodes ([Fig. 3F](#)), we used a binomial test
 779 to identify cells for which we could reject the null hypothesis that at least 95% of viral mRNA
 780 was derived from the more common viral barcode. We called IFN+ and ISG+ cells using the
 781 heuristic thresholds shown in [Fig. 3G](#) and [Fig. S6](#), respectively. We counted IFN mRNAs as any
 782 IFN- α , IFN- β , or IFN- λ transcripts. We counted ISG mRNAs as any of CCL5, IFIT1, ISG15, or Mx1.
 783 The plot in [Fig. 4](#) summarizes all of the genotypic information, and was created in substantial
 784 part using ggggenes (<https://github.com/wilkox/ggggenes>).

785 **Structural analysis of PB1 mutants.** To locate the PB1 mutations in the influenza A virus
 786 RNA polymerase structure relative to the template and active site in [Fig. 8A](#), we superposed the
 787 bat influenza A virus RNA polymerase structure (PDB 4WSB) (74), which shows the 3' terminus
 788 of the template on the surface of the RNA polymerase, with the influenza B virus transcription
 789 initiation complex (PDB 5MSG) (75), which shows the 3' terminus of the template in the template
 790 entry channel that leads towards the active site. The structural alignment was performed in
 791 Pymol 1.8.7 using motifs A and C.

792 **Experimental analysis of PB1 mutants.** For the experimental analysis of the PB1 mu-
 793 tants in [Fig. 8](#), we used plasmids pcDNA-PB1, pcDNA-PA, pcDNA-PB2, and pcDNA-NP, which
 794 encode the WSN proteins that compose the polymerase complex (94); pPolI-NA, which encodes
 795 the viral RNA for the WSN NA (94); and pcDNA-PB1a, which encodes an inactive version of
 796 the WSN PB1 polymerase protein (95). To construct plasmids expressing mutant PB1 proteins
 797 D27N and T677A, the plasmid pcDNA-PB1 was subjected to site-directed mutagenesis. PB1
 798 expression was analysed by western blot using antibody GTX125923 (GeneTex).

799 To analyze the activity of the PB1 mutants in cell culture, the plasmids expressing the
 800 WSN PA, PB2, NP and PB1 proteins were transfected into 293T cells together with the plasmid
 801 expressing the wildtype NA vRNA or a 246-nt long segment NP-based template (35). Twenty-
 802 four hours post transfection, the RNA was extracted using Trizol (Invitrogen), and the steady
 803 state RNA levels assessed using reverse transcription with 32P-labelled oligonucleotides against
 804 the viral RNA species and ribosomal 5S RNA as described previously (35, 96). 32P-derived
 805 signals were imaged using phosphorimaging on a Typhoon scanner and analysed using Prism
 806 (GraphPad). In all experiments, the apparent RNA levels were background corrected using the
 807 PB1a mutant and normalized to the 5S rRNA loading control.

808 To measure the induction of the IFN-beta promoter during these RNP reconstitution
 809 assays, they were carried out in the presence of a plasmid expressing Renilla luciferase from
 810 a CMV promoter and a plasmid expressing Firefly luciferase from the IFN-beta promoter (35).
 811 Twenty-four hours post transfection, cells were harvested, lysed and analysed using a DualGlo
 812 luciferase kit (Promega) according to the manufacturer's instructions. Samples were analysed
 813 using a GloMax (Promega).

815 **ACKNOWLEDGMENTS**

816 We thank Cole Trapnell, Jason Underwood, Robert Bradley, Daniel Stetson, Katherine
 817 Xue, and Hannah Itell for helpful suggestions. We thank Andy Marty and the Fred
 818 Hutch Genomics Core for performing the deep sequencing. This work was supported
 819 by the NIAID of the NIH under grant R01 AI127893 and a Burroughs Wellcome Fund
 820 Young Investigator in the Pathogenesis of Infectious Diseases grant to JDB. ABR was
 821 supported by a postdoctoral fellowship from the Damon Runyon Cancer Research
 822 Foundation (DRG-2227-15). JRK was supported by a Washington Research Foundation
 823 Undergraduate Research Fellowship and a Mary Gates undergraduate research schol-
 824 arship from the University of Washington. AtV was supported by joint Wellcome Trust
 825 and Royal Society grant 206579/Z/17/Z and Isaac Newton Trust grant 17.37(r). EE was
 826 supported by a Vice-Chancellor's scholarship from the University of Cambridge. JDB is
 827 an Investigator of the Howard Hughes Medical Institute. The funders had no role in
 828 study design, data collection and interpretation, or the decision to submit the work for
 829 publication.

830 **REFERENCES**

1. Stetson DB, Medzhitov R. Type I interferons in host defense. *Immunity* 2006; 25(3):373–381.
2. Honda K, Takaoka A, Taniguchi T. Type I interferon gene induction by the interferon regulatory factor family of transcription factors. *Immunity* 2006; 25(3):349–360.
3. Solov'ev V. The results of controlled observations on the prophylaxis of influenza with interferon. *Bull. World Heal. Organ.* 1969; 41(3-4-5):683.
4. Treanor JJ, Betts RF, Erb SM, Roth FK, Dolin R. Intranasally administered interferon as prophylaxis against experimentally induced influenza A virus infection in humans. *The J. Infect. Dis.* 1987; 156(2):379–383.
5. Beilharz MW, Cummins JM, Bennett AL. Protection from lethal influenza virus challenge by oral type 1 interferon. *Biochem. Biophys. Res. Commun.* 2007; 355(3):740–744.
6. Kugel D, Kochs G, Obojes K, Roth J, Kobinger GP, Kobasa D, Haller O, Staeheli P, Von Messling V. Intranasal administration of alpha interferon reduces seasonal influenza A virus morbidity in ferrets. *J. Virol.* 2009; 83(8):3843–3851.
7. Steel J, Staeheli P, Mubareka S, García-Sastre A, Palese P, Lowen AC. Transmission of pandemic H1N1 influenza virus and impact of prior exposure to seasonal strains or interferon treatment. *J. Virol.* 2010; 84(1):21–26.
8. La Gruta NL, Kedzierska K, Stambas J, Doherty PC. A question of self-preservation: immunopathology in influenza virus infection. *Immunol. Cell Biol.* 2007; 85(2):85–92.
9. Iwasaki A, Pillai PS. Innate immunity to influenza virus infection. *Nat. Rev. Immunol.* 2014; 14(5):315.
10. Kallfass C, Lienenklaus S, Weiss S, Staeheli P. Visualizing the Beta Interferon Response in Mice during Infection with Influenza A Viruses Expressing or Lacking Nonstructural Protein 1. *J. Virol.* 2013; 87(12):6925–6930.
11. Killip MJ, Jackson D, Pérez-Cidoncha M, Fodor E, Randall RE. Single-cell studies of IFN- β promoter activation by wild-type and NS1-defective influenza A viruses. *J. Gen. Virol.* 2017; 98(3):357–363.
12. Russell AB, Trapnell C, Bloom JD. Extreme heterogeneity of influenza virus infection in single cells. *eLife* 2018; 7:e32303.
13. Steuerman Y, Cohen M, Pesheh-Yaloz N, Valadarsky L, Cohn O, David E, Frishberg A, Mayo L, Bacharach E, Amit I, Gat-Viks I. Dissection of Influenza Infection In Vivo by Single-Cell RNA Sequencing. *Cell systems* 2018; 6:679–691.e4.
14. Sjaastad LE, Fay EJ, Fiege JK, Macchietto MG, Stone IA, Markman MW, Shen S, Langlois RA. Distinct antiviral signatures revealed by the magnitude and round of influenza virus replication in vivo. *Proc. Natl. Acad. Sci.* 2018; 115(38):9610–9615.
15. Heldt FS, Kupke SY, Dorl S, Reichl U, Frensing T. Single-cell analysis and stochastic modelling unveil large cell-to-cell variability in influenza A virus infection. *Nat. Commun.* 2015; 6:8938.
16. Wang C, Forst CV, Chou Tw, Geber A, Wang M, Hamou W, Smith M, Sebra R, Zhang B, Zhou B, et al. Cell-to-cell variation in defective virus expression and effects on host responses during influenza virus infection. *bioRxiv* 2018; DOI: 10.1101/364950.
17. McCrone JT, Woods RJ, Martin ET, Malosh RE, Monto AS, Lauring AS. Stochastic processes constrain the within and between host evolution of influenza virus. *eLife* 2018; 7:e35962.
18. Xue KS, Bloom JD. Reconciling disparate estimates of viral genetic diversity during human influenza infections. *Nat. Genet.* 2019; DOI: 10.1038/s41588-019-0349-3.
19. Varble A, Albrecht RA, Backes S, Crumiller M, Bouvier NM, Sachs D, García-Sastre A, et al. Influenza A virus transmission bottlenecks are defined by infection route and recipient host. *Cell Host & Microbe* 2014; 16(5):691–700.
20. Shalek AK, Satija R, Adiconis X, Gertner RS, Gaublomme JT, Raychowdhury R, Schwartz S, Yosef N, Malboeuf C, Lu D, et al. Single-cell transcriptomics reveals bimodality in expression and splicing in immune cells. *Nature* 2013; 498(7453):236–241.
21. Shalek AK, Satija R, Shuga J, Trombetta JJ, Gennert D, Lu D, Chen P, Gertner RS, Gaublomme JT, Yosef N, et al. Single cell RNA Seq reveals dynamic paracrine control of cellular variation. *Nature* 2014; 510(7505):363.
22. Wimmers F, Subedi N, van Buuringen N, Heister D, Vivé J, Beeren-Reinieren I, Woestenenk R, Dolstra H, Piruska A, Jacobs JF, et al. Single-cell analysis reveals that stochasticity and paracrine signaling control interferon-alpha production by plasmacytoid dendritic cells. *Nat. Commun.* 2018; 9(1):3317.
23. Bhushal S, Wolfsmüller M, Selvakumar T, Kemper L, Wirth D, Hornef M, Hauser H, Köster M. Cell Polarization and Epigenetic Status Shape the Heterogeneous Response to Type III Interferons in Intestinal Epithelial Cells. *Front. Immunol.* 2017; 8:671–671.
24. García-Sastre A, Egorov A, Matassov D, Brandt S, Levy DE, Durbin JE, Palese P, Muster T. Influenza A virus lacking the NS1 gene replicates in interferon-deficient systems. *Virology* 1998; 252(2):324–330.
25. Hale BG, Randall RE, Ortín J, Jackson D. The multifunctional NS1 protein

- of influenza A viruses. *J. Gen. Virol.* 2008; 89(10):2359–2376.
26. Hayashi T, MacDonald LA, Takimoto T. Influenza A virus protein PA-X contributes to viral growth and suppression of the host antiviral and immune responses. *J. Virol.* 2015; 89(12):6442–6452.
 27. Vreede FT, Chan AY, Sharps J, Fodor E. Mechanisms and functional implications of the degradation of host RNA polymerase II in influenza virus infected cells. *Virology* 2010; 396(1):125–134.
 28. Dudek SE, Wixler L, Nordhoff C, Nordmann A, Anhlan D, Wixler V, Ludwig S. The influenza virus PB1-F2 protein has interferon antagonistic activity. *Biol. Chem.* 2011; 392(12):1135–1144.
 29. Killip MJ, Fodor E, Randall RE. Influenza virus activation of the interferon system. *Virus research* 2015; 209:11–22.
 30. Parvin JD, Moscona A, Pan W, Leider J, Palese P. Measurement of the mutation rates of animal viruses: influenza A virus and poliovirus type 1. *J. Virol.* 1986; 59(2):377–383.
 31. Suárez P, Valcárcel J, Ortín J. Heterogeneity of the mutation rates of influenza A viruses: isolation of mutator mutants. *J. Virol.* 1992; 66(4):2491–2494.
 32. Suárez-López P, Ortín J. An estimation of the nucleotide substitution rate at defined positions in the influenza virus haemagglutinin gene. *J. Gen. Virol.* 1994; 75(2):389–393.
 33. Bloom JD. An experimentally determined evolutionary model dramatically improves phylogenetic fit. *Mol. Biol. Evol.* 2014; 31(8):1956–1978.
 34. Pauly MD, Procaro MC, Lauring AS. A novel twelve class fluctuation test reveals higher than expected mutation rates for influenza A viruses. *eLife* 2017; 6:e26437.
 35. te Velthuis A, Long J, Bauer DL, Fan R, Yen HL, Sharps J, Siegers J, Killip M, French H, Oliva-Martin MJ, Randall R, de Wit E, van Riel D, Poon L, Fodor E. Mini viral RNAs act as innate immune agonists during influenza virus infection. *Nat. Microbiol.* 2018; 3(11):1234–1242.
 36. Du Y, Xin L, Shi Y, Zhang TH, Wu NC, Dai L, Gong D, Brar G, Shu S, Luo J, Reiley W, Tseng YW, Bai H, Wu TT, Wang J, Shu Y, Sun R. Genome-wide identification of interferon-sensitive mutations enables influenza vaccine design. *Science* 2018; 359(6373):290–296.
 37. Pérez-Cidoncha M, Killip M, Oliveros J, Asensio V, Fernández Y, Ben-goechea J, Randall R, Ortín J. An unbiased genetic screen reveals the polygenic nature of the influenza virus anti-interferon response. *J. Virol.* 2014; 88(9):4632–4646.
 38. Baum A, Sachidanandam R, García-Sastre A. Preference of RIG-I for short viral RNA molecules in infected cells revealed by next-generation sequencing. *Proc. Natl. Acad. Sci.* 2010; 107(37):16303–16308.
 39. Tapia K, Kim Wk, Sun Y, Mercado-López X, Dunay E, Wise M, Adu M, López CB. Defective viral genomes arising in vivo provide critical danger signals for the triggering of lung antiviral immunity. *PLoS Pathog.* 2013; 9(10):e1003703.
 40. Boergeling Y, Rozhdestvensky TS, Schmolke M, Resa-Infante P, Robeck T, Randau G, Wolff T, Gabriel G, Brosius J, Ludwig S. Evidence for a novel mechanism of influenza virus-induced type I interferon expression by a defective RNA-encoded protein. *PLoS Pathog.* 2015; 11(5):e1004924.
 41. Dimmock NJ, Easton AJ. Cloned defective interfering influenza RNA and a possible pan-specific treatment of respiratory virus diseases. *Viruses* 2015; 7(7):3768–3788.
 42. Liu G, Lu Y, Liu Q, Zhou Y. Inhibition of Ongoing Influenza A Virus Replication Reveals Different Mechanisms of RIG-I Activation. *J. Virol.* 2019; 93:DOI 10.1128/JVI.02066–18.
 43. Brooke CB, Ince WL, Wrammert J, Ahmed R, Wilson PC, Bennink JR, Yewdell JW. Most influenza A virions fail to express at least one essential viral protein. *J. Virol.* 2013; 87:3155–3162.
 44. Guo F, Li S, Caglar MU, Mao Z, Liu W, Woodman A, Arnold JJ, Wilke CO, Huang TJ, Cameron CE. Single-cell virology: on-chip investigation of viral infection dynamics. *Cell Reports* 2017; 21(6):1692–1704.
 45. Zanini F, Pu SY, Bekerman E, Einav S, Quake SR. Single-cell transcriptional dynamics of flavivirus infection. *eLife* 2018; 7:e32942.
 46. Zanini F, Robinson M, Croote D, Sahoo MK, Sanz AM, Ortiz-Lasso E, Albornoz LL, Suarez FR, Montoya JG, Pinsky BA, Quake S, Einav S. Virus-inclusive single cell RNA sequencing reveals molecular signature predictive of progression to severe dengue infection. *PNAS* 2018; DOI: 10.1073/pnas.1813819115.
 47. Saikia M, Burnham P, Keshavjee SH, Wang MF, Heyang M, Moral-Lopez P, Hinchman MM, Danko CG, Parker JS, De Vlaminck I. Simultaneous multiplexed amplicon sequencing and transcriptome profiling in single cells. *Nat. Methods* 2019; 16:59–62.
 48. O’Neal JT, Upadhyay AA, Wolabaugh A, Patel NB, Bosinger SE, Suthar MS. West Nile virus-inclusive single-cell RNA sequencing reveals heterogeneity in the type I interferon response within single cells. *J. Virol.* 2019; DOI: 10.1128/JVI.01778-18.
 49. Bonini C, Ferrari G, Verzeletti S, Servida P, Zappone E, Ruggieri L, Ponzoni M, Rossini S, Mavilio F, Traversari C, Bordignon C. HSV-TK gene transfer into donor lymphocytes for control of allogeneic graft-versus-leukemia. *Science* 1997; 276(5319):1719–1724.
 50. Ruggieri L, Auti A, Salomoni M, Zappone E, Ferrari G, Bordignon C. Cell-surface marking of CD34+-restricted phenotypes of human hematopoietic progenitor cells by retrovirus-mediated gene transfer. *Hum. Gene Ther.* 1997; 8(13):1611–1623.
 51. Strahle L, Garcin D, Kolakofsky D. Sendai virus defective-interfering genomes and the activation of interferon-beta. *Virology* 2006; 351(1):101–111.
 52. Hoffmann E, Neumann G, Kawaoka Y, Hobom G, Webster RG. A DNA transfection system for generation of influenza A virus from eight plasmids. *Proc. Natl. Acad. Sci.* 2000; 97(11):6108–6113.
 53. Xue J, Chambers BS, Hensley SE, López CB. Propagation and characterization of influenza virus stocks that lack high levels of defective viral genomes and hemagglutinin mutations. *Front. Microbiol.* 2016; 7:326.
 54. Zheng GX, Terry JM, Belgrader P, Ryvkin P, Bent ZW, Wilson R, Ziraldo SB, Wheeler TD, McDermott GP, Zhu J, et al. Massively parallel digital transcriptional profiling of single cells. *Nat. Commun.* 2017; 8:14049.
 55. Robertson J, Schubert M, Lazzarini R. Polyadenylation sites for influenza virus mRNA. *J. Virol.* 1981; 38(1):157–163.
 56. Koppstein D, Ashour J, Bartel DP. Sequencing the cap-snatching repertoire of H1N1 influenza provides insight into the mechanism of viral transcription initiation. *Nucleic Acids Res.* 2015; 43(10):5052–5064.
 57. Travers KJ, Chin CS, Rank DR, Eid JS, Turner SW. A flexible and efficient template format for circular consensus sequencing and SNP detection. *Nucleic Acids Res.* 2010; 38(15):e159.
 58. Bloom JD. Estimating the frequency of multiplets in single-cell RNA sequencing from cell-mixing experiments. *PeerJ* 2018; 6:e5578.
 59. Haque A, Engel J, Teichmann SA, Lönnberg T. A practical guide to single-cell RNA-sequencing for biomedical research and clinical applications. *Genome Medicine* 2017; 9(1):75.
 60. Dou D, Hernández-Neuta I, Wang H, Östbye H, Qian X, Thiele S, Resa-Infante P, Kouassi NM, Sender V, Henrich K, Mellroth P, Henriques-Normark B, Gabriel G, Nilsson M, Daniels R. Analysis of IAV replication and co-infection dynamics by a versatile RNA viral genome labeling method. *Cell Reports* 2017; 20(1):251–263.
 61. Jacobs NT, Onuoha NO, Antia A, Antia R, Steel J, Lowen AC. Incomplete influenza A virus genomes are abundant but readily complemented during spatially structured viral spread. *bioRxiv* 2019; DOI 10.1101/529065.
 62. Hatada E, Hasegawa M, Mukaiyama J, Shimizu K, Fukuda R. Control of influenza virus gene expression: quantitative analysis of each viral RNA species in infected cells. *The J. Biochem.* 1989; 105(4):537–546.
 63. Aguilera ER, Erickson AK, Jesudhasan PR, Robinson CM, Pfeiffer JK. Plaques formed by mutagenized viral populations have elevated coin-

- fection frequencies. *mBio* 2017; 8(2):e02020-16.
64. Combe M, Garijo R, Geller R, Cuevas JM, Sanjuán R. Single-cell analysis of RNA virus infection identifies multiple genetically diverse viral genomes within single infectious units. *Cell Host & Microbe* 2015; 18(4):424-432.
 65. Dhir A, Dhir S, Borowski LS, Jimenez L, Teitel M, Rötig A, Crow YJ, Rice GI, Duffy D, Tamby C, et al. Mitochondrial double-stranded RNA triggers antiviral signalling in humans. *Nature* 2018; 560(7717):238-242.
 66. Benitez AA, Panis M, Xue J, Varble A, Shim JV, Frick AL, López CB, Sachs D, et al. In vivo RNAi screening identifies MDA5 as a significant contributor to the cellular defense against influenza A virus. *Cell reports* 2015; 11(11):1714-1726.
 67. Chiang J, Sparre K, Lässig C, Huang T, Osterrieder N, Hopfner K, Gack M, et al. Viral unmasking of cellular 5S rRNA pseudogene transcripts induces RIG-I-mediated immunity. *Nat. Immunol.* 2018; 19(1):53-62.
 68. Maaten Lvd, Hinton G. Visualizing data using t-SNE. *J. Mach. Learn. Res.* 2008; 9(Nov):2579-2605.
 69. Xu H, DiCarlo J, Satya RV, Peng Q, Wang Y. Comparison of somatic mutation calling methods in amplicon and whole exome sequence data. *BMC Genomics* 2014; 15(1):244.
 70. Cibulskis K, Lawrence MS, Carter SL, Sivachenko A, Jaffe D, Sougnez C, Gabriel S, Meyerson M, Lander ES, Getz G. Sensitive detection of somatic point mutations in impure and heterogeneous cancer samples. *Nat. Biotechnol.* 2013; 31(3):213-222.
 71. Gini C. Measurement of inequality of incomes. *The Econ. J.* 1921; 31(121):124-126.
 72. Fujii Y, Goto H, Watanabe T, Yoshida T, Kawaoka Y. Selective incorporation of influenza virus RNA segments into virions. *Proc. Natl. Acad. Sci.* 2003; 100(4):2002-2007.
 73. Marsh GA, Hatami R, Palese P. Specific residues of the influenza A virus hemagglutinin viral RNA are important for efficient packaging into budding virions. *J. Virol.* 2007; 81(18):9727-9736.
 74. Reich S, Guilligay D, Pflug A, Malet H, Berger I, Crépin T, Hart D, Lunardi T, Nanao M, Ruigrok RW, et al. Structural insight into cap-snatching and RNA synthesis by influenza polymerase. *Nature* 2014; 516(7531):361-366.
 75. Reich S, Guilligay D, Cusack S. An in vitro fluorescence based study of initiation of RNA synthesis by influenza B polymerase. *Nucleic Acids Res.* 2017; 45(6):3353-3368.
 76. Zhu Y, Yongky A, Yin J. Growth of an RNA virus in single cells reveals a broad fitness distribution. *Virology* 2009; 385(1):39-46.
 77. Schulte M, Andino R. Single-cell analysis uncovers extensive biological noise in poliovirus replication. *J. Virol.* 2014; 88(11):6205-6212.
 78. Akpinar F, Timm A, Yin J. High-throughput single-cell kinetics of virus infections in the presence of defective interfering particles. *J. Virol.* 2016; 90(3):1599-1612.
 79. Gupta I, Collier PG, Haase B, Mahfouz A, Joglekar A, Floyd T, Koopmans F, Barres B, Smit AB, Sloan S, et al. Single-cell isoform RNA sequencing (SciSOR-Seq) across thousands of cells reveals isoforms of cerebellar cell types. *Nat. Biotechnol.* 2018; 36:1197-1202.
 80. O'Connell RM, Balazs AB, Rao DS, Kivork C, Yang L, Baltimore D. Lentiviral vector delivery of human interleukin-7 (hIL-7) to human immune system (HIS) mice expands T lymphocyte populations. *PLoS One* 2010; 5(8):e12009.
 81. Kim JH, Lee SR, Li LH, Park HJ, Park JH, Lee KY, Kim MK, Shin BA, Choi SY. High cleavage efficiency of a 2A peptide derived from porcine teschovirus-1 in human cell lines, zebrafish and mice. *PloS One* 2011; 6(4):e18556.
 82. Reed LJ, Muench H. A simple method of estimating fifty per cent endpoints. *Am. J. Epidemiol.* 1938; 27(3):493-497.
 83. Doud MB, Hensley SE, Bloom JD. Complete mapping of viral escape from neutralizing antibodies. *PLoS Pathog.* 2017; 13(3):e1006271.
 84. Boers SA, Hays JP, Jansen R. Micelle PCR reduces chimera formation in 16S rRNA profiling of complex microbial DNA mixtures. *Sci. Reports* 2015; 5:14181.
 85. Killip MJ, Smith M, Jackson D, Randall RE. Activation of the Interferon Induction Cascade by Influenza A Viruses Requires Viral RNA Synthesis and Nuclear Export. *J. Virol.* 2014; 88(8):3942-3952.
 86. Hirst GK. The quantitative determination of influenza virus and antibodies by means of red cell agglutination. *J. Exp. Medicine* 1942; 75(1):49-64.
 87. Bloom JD, Gong LI, Baltimore D. Permissive Secondary Mutations Enable the Evolution of Influenza Oseltamivir Resistance. *Science* 2010; 328(5983):1272-1275.
 88. Köster J, Rahmann S. Snakemake—a scalable bioinformatics workflow engine. *Bioinformatics* 2012; 28(19):2520-2522.
 89. Li H. Minimap2: pairwise alignment for nucleotide sequences. *Bioinformatics* 2018; 1:7.
 90. Bloom JD. Software for the analysis and visualization of deep mutational scanning data. *BMC Bioinforma.* 2015; 16(1):168.
 91. Huber W, Carey VJ, Gentleman R, Anders S, Carlson M, Carvalho BS, Bravo HC, Davis S, Gatto L, Girke T, Gottardo R, Hahne F, Hansen KD, Irizarry RA, Lawrence M, Love MI, MacDonald J, Obenchain V, Oles AK, Pages H, Reyes A, Shannon P, Smyth GK, Tenenbaum D, Waldron L, Morgan M. Orchestrating high-throughput genomic analysis with Bioconductor. *Nat. Methods* 2015; 12(2):115.
 92. Qiu X, Mao Q, Tang Y, Wang L, Chawla R, Pliner HA, Trapnell C. Reversed graph embedding resolves complex single-cell trajectories. *Nat. Methods* 2017; 14(10):979.
 93. Trapnell C, Cacchiarelli D, Grimsby J, Pokharel P, Li S, Morse M, Lennon NJ, Livak KJ, Mikkelsen TS, Rinn JL. The dynamics and regulators of cell fate decisions are revealed by pseudotemporal ordering of single cells. *Nat. Biotechnol.* 2014; 32(4):381.
 94. Fodor E, Crow M, Mingay LJ, Deng T, Sharps J, Fechter P, Brownlee GG. A single amino acid mutation in the PA subunit of the influenza virus RNA polymerase inhibits endonucleolytic cleavage of capped RNAs. *J. Virol.* 2002; 76(18):8989-9001.
 95. Vreede FT, Jung TE, Brownlee GG. Model suggesting that replication of influenza virus is regulated by stabilization of replicative intermediates. *J. Virol.* 2004; 78(17):9568-9572.
 96. te Velthuis AJ, Robb NC, Kapanidis AN, Fodor E. The role of the priming loop in influenza A virus RNA synthesis. *Nat. Microbiol.* 2016; 1(5):16029.
 97. Boni MF, Zhou Y, Taubenberger JK, Holmes EC. Homologous recombination is very rare or absent in human influenza A virus. *J. Virol.* 2008; 82(10):4807-4811.

831 SUPPLEMENTAL MATERIAL

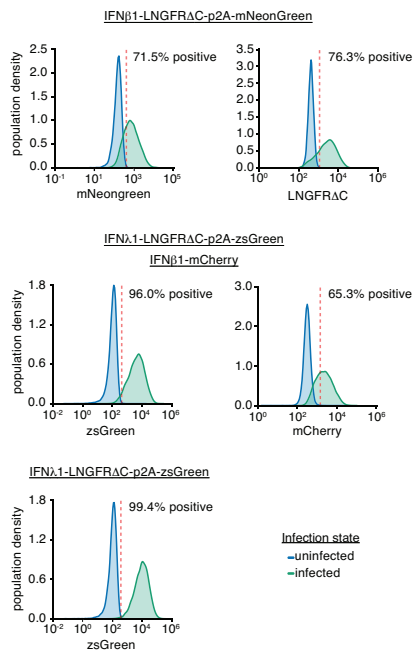
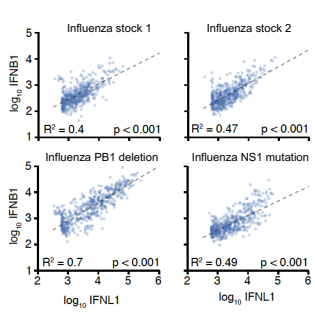
A**B**

FIG S1 Validation of reporter cell lines (Fig. 1A) to identify IFN+ cells. (A) To validate the IFN reporter cell lines, they were infected at high MOI with the Cantell strain of Sendai virus, which strongly activates IFN expression (51). The name of each of reporter cell line is indicated at the top of each row of plots. At 13 hours post-infection, activation of the IFN reporter was then monitored by flow cytometry using the marker indicated at the bottom of each plot (either a fluorescent protein or antibody staining for the cell-surface LNGFRΔC using a PE-conjugated anti-LNGFR antibody from Miltenyi Biotec). Sendai infection efficiently activated the IFN reporter in all cases, with the strongest signal from the IFN- λ reporter driving ZsGreen. (B) The type I and type III IFN reporters are highly correlated in their activation. An A549 cell line was generated by transduction with both the IFN- β and IFN- λ reporters driving expression of mCherry and ZsGreen, respectively. The cells were then infected with two different stocks of “wild-type” WSN influenza, or stocks with a deletion in PB1 or stop codons in NS1 (described later in the paper). After 13 hours, cells were analyzed by flow cytometry. Cells positive for either fluorescent reporter were further analyzed. As shown in the FACS plots, expression of the *IFNB1* and *IFNL1* reporters is highly correlated in all cases.

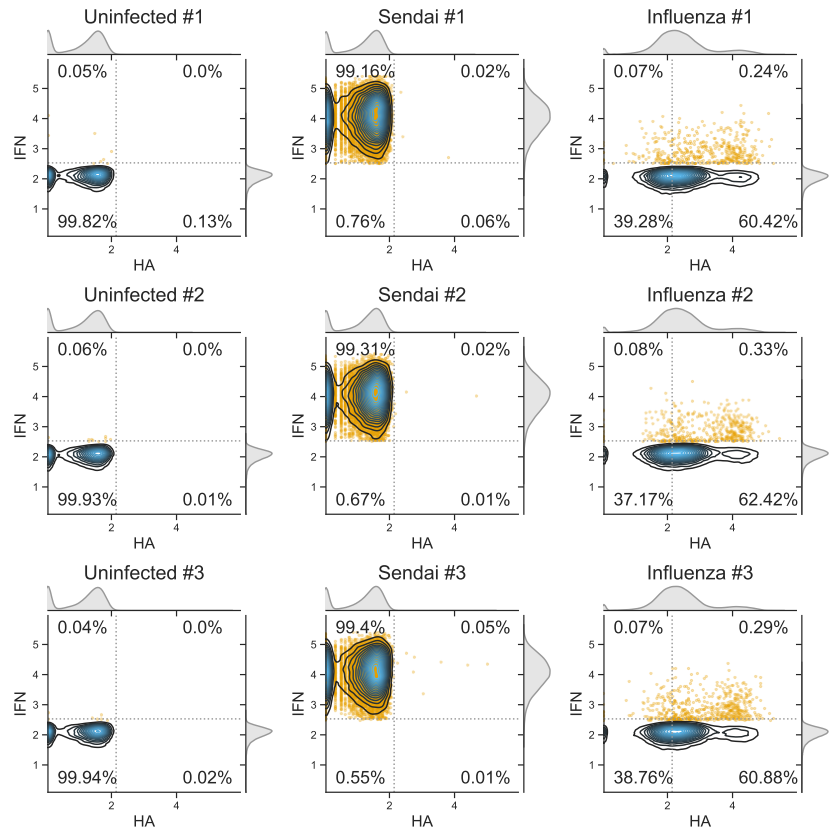


FIG S2 Flow cytometry data for Fig. 1B. The A549 cells with the *IFNL1* reporter driving LNGFRΔC-ZsGreen were not infected, infected with saturating amounts of the Cantell strain of Sendai virus-(51), or infected the same stock of influenza virus used in the single-cell experiment at a target MOI of 0.3. After 13 hours, the cells were stained for expression of HA protein and analyzed by FACS for HA and expression of the ZsGreen driven by the *IFNL1* reporter. Each condition was done in triplicate. The contour plots show the density of all cells, and all IFN+ cells are also indicated by orange dots. Cells were classified as HA+ or IFN+ based on gates set to put 0.05% of the uninfected cells in these populations. For the influenza-infected cells, the percentage IFN+ was calculated only among the HA+ cells (since these are the ones that are infected). For the uninfected and Sendai-virus infected, the percentage IFN+ was calculated among all cells, since these cells do not express HA.

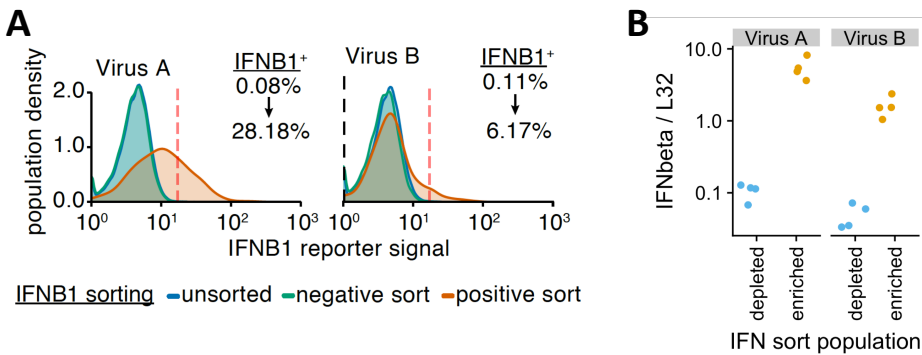


FIG S3 Example MACS enrichments of IFN+ influenza-infected cells. A549 cells with the *IFNB1* LNGFRΔC-mNeonGreen reporter were infected with wild-type WSN influenza (two different viral stocks) at a target MOI of 0.1 TCID50 per cell. After infection had proceeded for 12 hours, the cells were twice magnetically sorted for LNGFRΔC expression over magnetic columns as detailed in the methods for the single-cell sequencing experiment. (A) After sorting, the populations were analyzed by flow cytometry for IFN expression using the mNeonGreen fluorescent protein. The plots show the distribution of fluorescence in the original population, the flow-through from the first column, and the MACS-sorted positive population after two columns. As indicated by the percentages shown for the original and MACS-sorted population, this process led to substantial enrichment in IFN+ cells. We expect that the IFN sorting for the actual single-cell sequencing led to similar enrichment, although we could not directly quantify this as the sorted cells in that case were immediately used for the sequencing and so could not be analyzed by flow cytometry. (B) Analysis of expression of *IFNB1* (relative to the housekeeping gene *L32*) by qPCR in the positive (IFN enriched) and negative (IFN depleted) populations from panel (A). The qPCR validates a roughly 50- to 100-fold enrichment in total *IFNB1* expression. The qPCR was performed in quadruplicate (hence the four points for each sample).

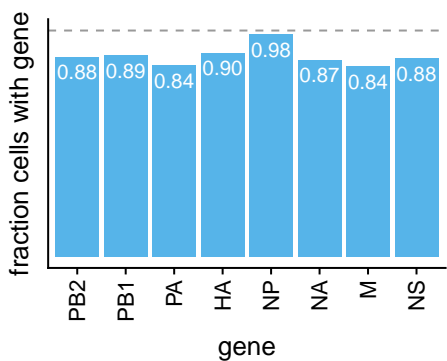


FIG S4 The fraction of infected cells that are called as expressing each viral gene. The gray dashed line is at one (the fraction that would be observed if all viral genes are expressed in all infected cells). Each viral gene is detected in ~80-90% of the infected cells, roughly in line with prior estimates (43, 15, 60, 12). The exception is NP, which is detected in virtually all infected cells. The much higher frequency of detecting NP could reflect a biological phenomenon, but we suspect it is more likely that cells lacking NP tend to have much lower viral gene expression overall and so are not reliably called as being infected in our experiments because the number of viral mRNAs is below the detection limit.

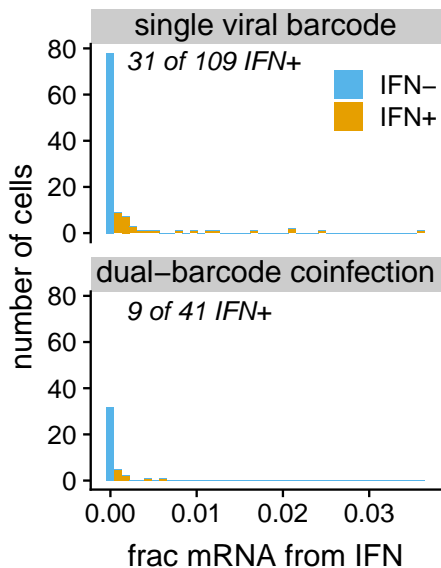


FIG S5 The correlation—There is no association between viral co-infection and expression of IFN in our experiments using low MOI infections with a relatively “pure” viral stock. Histograms show the fraction of all cellular mRNA derived from type I and type III IFN in the A549 among cells in our single-cell transcriptomics expressing viral mRNA from just a single viral barcode variant, or cells expressing viral mRNA from both the wildtype and synonymously barcoded viral variants. Each point represents one cell. The plots are faceted by whether dual-barcode cells represent known co-infections, whereas the single-barcode cells are called as represent a mix of singly infected cells and co-infections with the Pearson correlation coefficient is shown same viral barcode. Because type I and type III IFN expression are highly correlated, for There is no significant difference in the remainder frequency of IFN induction among the paper we group them together and refer to their combined expression as the level two classes of IFN cells ($P = 0.53$, Fisher’s exact test).

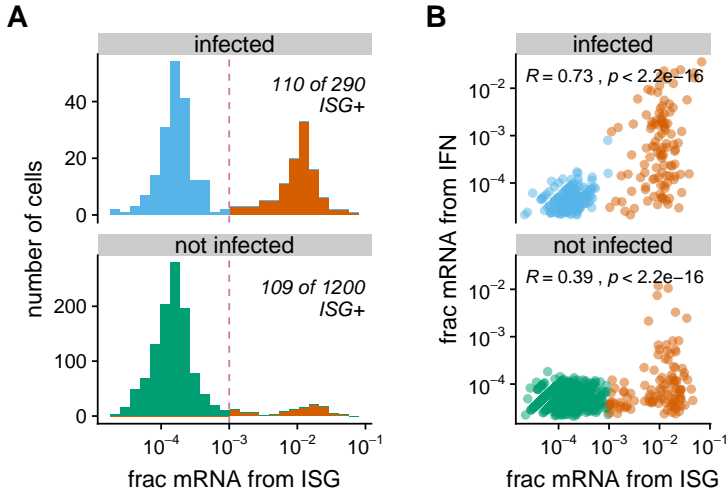


FIG S6 Expression of ISGs in single infected and uninfected cells. For each cell, we quantified ISG expression as the total fraction of cellular mRNAs derived from four prototypical ISGs (IFIT1, ISG15, CCL5, and Mx1). (A) The histograms show the distribution of ISG expression taken across infected (top) and uninfected (bottom) cells. We heuristically classify as ISG+ cells with $> 10^{-3}$ of their cellular mRNA from ISGs, and color these cells red. Comparison to Fig. 3G shows that substantially more cells are ISG+ than IFN+, both among infected and uninfected cells. This is probably because paracrine signaling can induce ISG expression in cells that are not themselves expressing IFN^(1,2). (B) Correlation between the fraction of cellular mRNA derived from IFN and ISGs. Each point represents one cell, and the Pearson correlation coefficient is shown. IFN and ISG expression are more correlated for infected than uninfected cells, probably because in the latter the ISG expression is more often due to paracrine signaling that does not induce expression of IFN itself. Among both the infected and uninfected populations, there are many cells with high expression of ISGs and little expression of IFN, but no cells that express high levels of IFN without also substantially expressing ISGs.

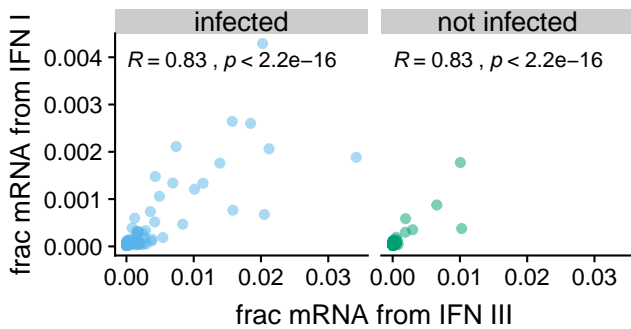


FIG S7 The correlation between the fraction of cellular mRNA derived from type I and type III IFN in the A549 cells in our single-cell transcriptomics. Each point represents one cell. The plots are faceted by whether the cells are called as infected, and the Pearson correlation coefficient is shown. Because type I and type III IFN expression are highly correlated, for the remainder of the paper we group them together and refer to their combined expression as the level of IFN.

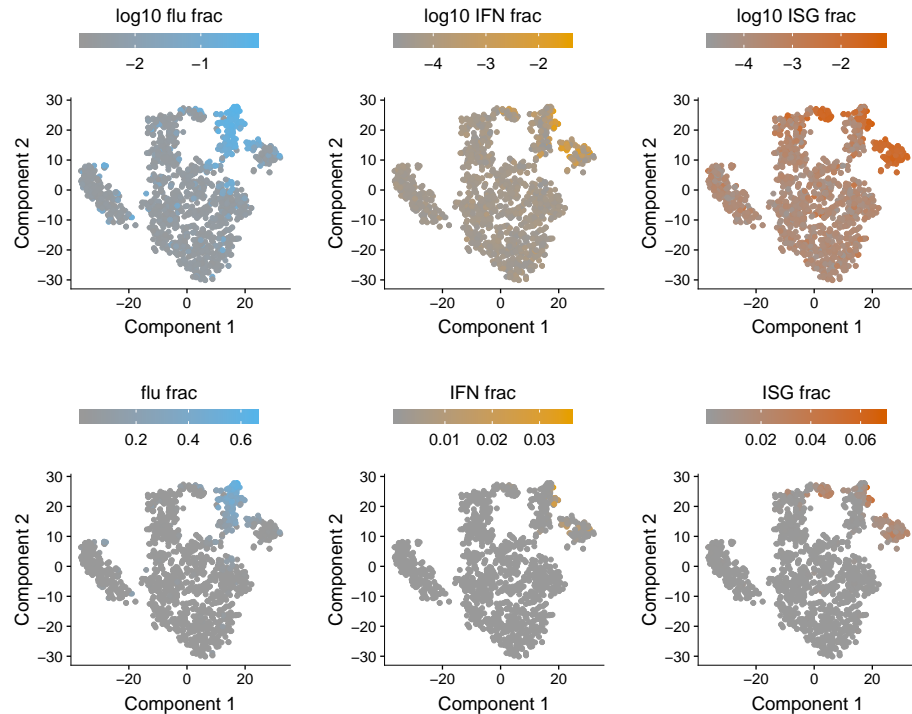


FIG S8 Unsupervised t-SNE clustering shows that cell-to-cell variation in expression of influenza, IFN, and ISG transcripts substantially contributes to the structure of the data. To generate an unbiased representation of the factors that distinguished the transcriptomes of the cells in our experiments, we used unsupervised t-SNE clustering (68) as implemented in Monocle (92, 93) to generate a two-dimensional representation of the data. In the t-SNE plot, each point is a different cell, and cells with similar transcriptomes are closer together. Each panel shows the same t-SNE plot, but the cells are colored differently in each panel based on the amount of viral, IFN, or ISG mRNA, shown on a log (top) or linear (bottom) scale. As is clear from this plot, expression of influenza, IFN, and ISG genes contributes substantially to the structure of the data, since cells with high expression of these genes clearly group together.

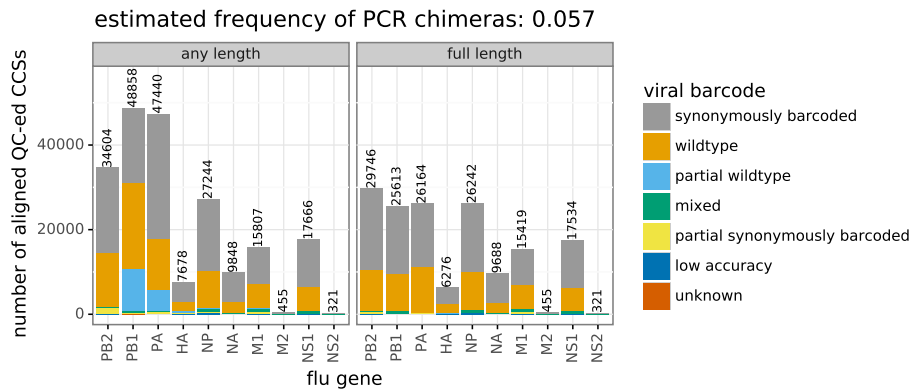


FIG S9 The number of PacBio CCSs that passed quality-control steps and aligned to an influenza virus gene. These sequences were obtained using several PacBio runs, most of which were intentionally loaded with different amounts of the various viral genes to increase coverage on genes that were needed in order to obtain the full sequences of virions infecting cells (see [File S7](#)). Because of this unequal loading and the inherently different PCR amplification efficiencies of different viral genes, unlike the transcriptomic data in [Fig. 3](#), the numbers of CCSs for different genes should *not* be taken as an indicator of their abundance in the infected cells. Especially for the polymerase genes (PB2, PB1, and PA), many CCSs corresponded to genes with internal deletions, since these shorter forms of the genes were preferentially amplified during PCR. Therefore, the plot is faceted by the number of CCSs for any length of the gene, and for full-length genes. Note that the disproportionate sequencing of the shorter internally deleted genes does not greatly affect the genotype calling in [Fig. 4](#) since UMIs were used to collapse sequences derived from the same cDNA, and cell barcodes were used to collapse sequences from the same cell. The bars in the plot are colored by whether the sequence is derived from the wild-type viral variant, the synonymously barcoded viral variant, or represents a mixed-barcode molecule (see panel B). From the frequencies of these different forms, we estimate [\(58\)](#) that 5.7% of molecules are chimeric due to PCR strand exchange. About half of these PCR chimeras could be identified by the presence of mixed viral barcodes and removed from subsequent analyses, leaving ~3% un-identified chimeras. For some molecules (mostly polymerase genes with internal deletions) one of the barcode sites was deleted from the molecule and so the barcode identity could only be partially called. A negligible number of molecules have low-accuracy sequence or unexpected nucleotide identities at the sites of the viral barcodes.

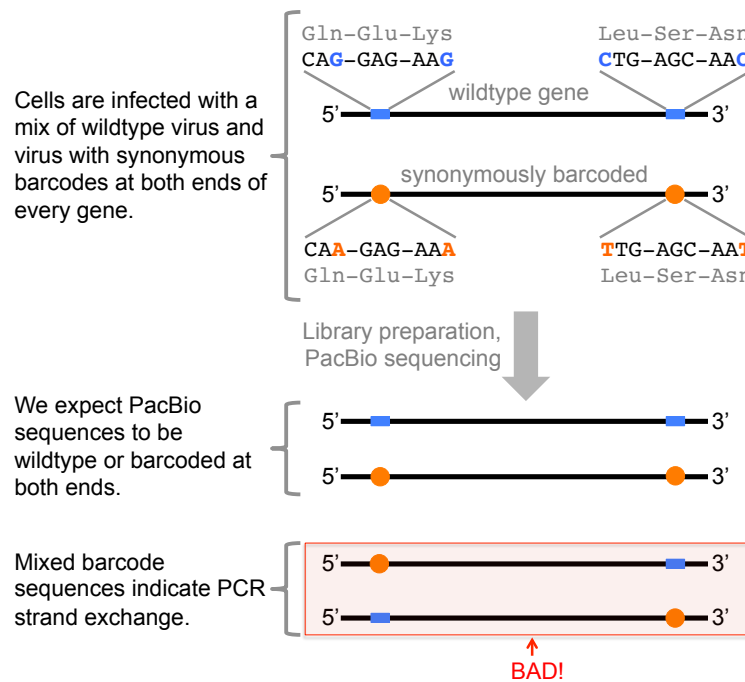


FIG S10 Strategy for detecting strand exchange during sequencing of full-length viral genes. The library preparation for PacBio sequencing of the cDNA for the full-length viral genes required many cycles of PCR. A major concern is that strand exchange during this PCR could scramble mutations and 10X cell barcodes / UMIs from different molecules. We detect PCR strand exchange by leveraging the fact that our cells were infected with a mix of wild-type virus and virus carrying synonymous barcodes near both termini of each gene. If there is no strand exchange, all molecules should either be wild-type or have the synonymous barcoding mutations at *both* termini. Strand exchange will create some molecules that have wild-type nucleotides at one termini and synonymous barcoding mutations at the other termini. Fig. S9 shows the frequencies with which these different types of molecules were observed during the PacBio sequencing. Note that since the rate of homologous recombination in influenza virus is negligible (97), such mixed-barcode molecules are *not* expected to be generated naturally during co-infection.

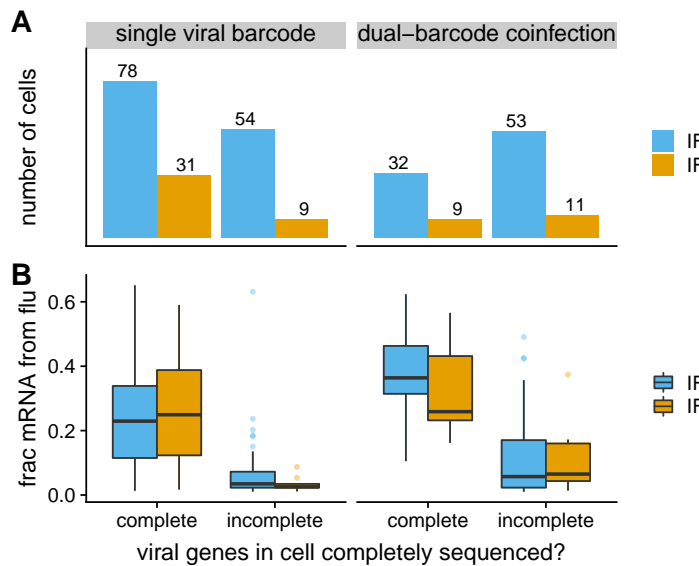


FIG S11 Number of cells for which we could determine the full sequences of all genes expressed by the infecting virion(s). (A) We could call the complete genotypes of the infecting virion(s) for the majority of cells infected with just a single viral barcode variant, but only a minority of cells co-infected with both viral barcodes. (B) The cells for which we could call complete viral genotypes tended to have higher expression of viral mRNA than cells for which we could not call complete genotypes. Both facts make sense. Cells with more viral mRNA are more likely to have their viral cDNA captured in the PacBio sequencing, which only captures a small fraction of the total transcripts identified by the 3'-end sequencing transcriptomic sequencing. The lower calling rate for dual-barcode co-infections is probably because these co-infections have more viral genes that must be sequenced (potentially a copy of each viral gene from each viral variant), increasing the chances that one of these genes is missed by the PacBio sequencing. An important implication of this plot is that the cells for which we call complete viral genotypes are *not* a random subsampling of all infected cells in the experiment, but are rather enriched for cells that have high levels of viral mRNA and do not have dual-barcode viral infections. Note also that this plot is limited to the cells that were called as infected (Fig. 3C) and could clearly be classified as IFN- or IFN+ (Fig. 3G).

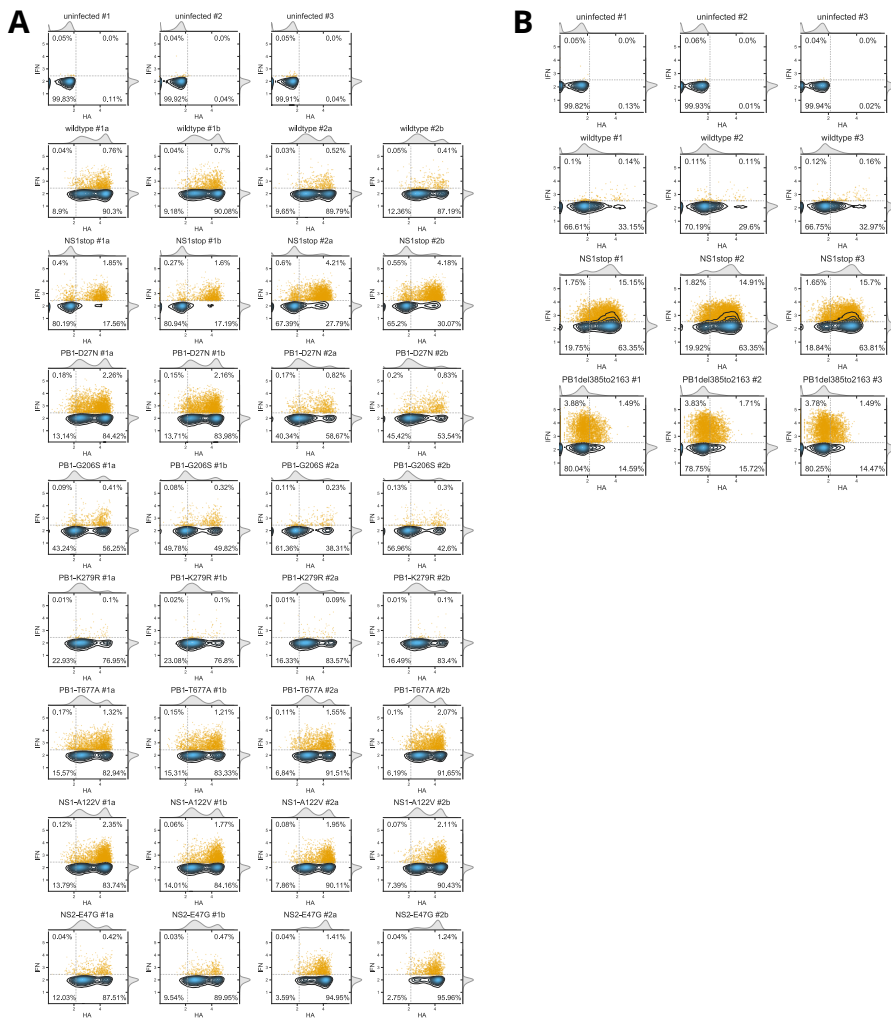


FIG S12 Flow cytometry data for Fig. 6. (A) Data for Fig. 6A. A549 cells with the *IFNL1* reporter driving LNGFR Δ -ZsGreen were infected with stocks of the indicated mutant. After 13 hours, cells were stained for HA protein and analyzed by FACS. Contour plots show density of all cells, and IFN+ cells are also indicated by orange dots. Cells were classified as HA+ or IFN+ based on gates set to put 0.05% of uninfected cells in these populations. For infected cells, the percentage IFN+ was calculated among the HA+ cells (since these are the ones that are infected). For uninfected cells, the percentage IFN+ was calculated among all cells, since uninfected cells do not express HA. For each viral mutant, two independent stocks were assayed in duplicate (i.e., #1a and #1b are one viral stock, and #2a and #2b are the other). The infections with replicate #1 of the wild-type virus were performed at an MOI of 0.1 as determined by TCID50, and all other viruses were infected at an equivalent particle number as determined by HI assay. (B) Data for Fig. 6B. The virus with the deletion in PB1 cannot be normalized by HA expression since it expresses less HA due to the lack of secondary transcription. Therefore, all cells were infected at an equivalent MOI of 0.3 as determined by TCID50 on MDCK-SIAT1 cells for wild type and NS1stop, and on MDCK-SIAT1 cells expressing PB1-~~(87)~~ for PB1del385to2163. Fig. S13 shows that at these equivalent TCID50s, all variants had similar amounts of transcriptionally active virus in the absence of secondary transcription. The percent IFN+ was calculated for *all* cells (HA+ and HA-) since that is a more fair comparison for PB1del385to2163.

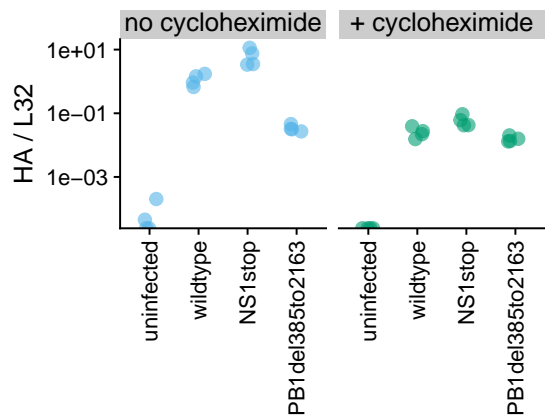


FIG S13 Validation that the infections in Fig. 6B and Fig. S12B were performed at similar doses of virions capable of initiating primary transcription. In this experiment, A549 cells were infected at MOI of 0.4 (based on TCID₅₀ as described in Fig. S12B), and then after 8 hours mRNA was harvested for qPCR on oligo-dT primed reverse transcription products. The y-axis shows the ratio of viral HA mRNA to the housekeeping gene L32. These infections were performed in the presence or absence of 50 µg/ml cycloheximide, which blocks protein synthesis and hence secondary transcription by newly synthesized viral proteins (85). In the absence of cycloheximide, the viruses with deletions in PB1 produced less viral mRNA presumably because they could not produce PB1 protein for secondary transcription. But in the presence of cycloheximide, all viruses produced similar amounts of viral mRNA, indicating that the dose of particles active for primary transcription is roughly equivalent across variants. Each measurement was performed in quadruplicate.

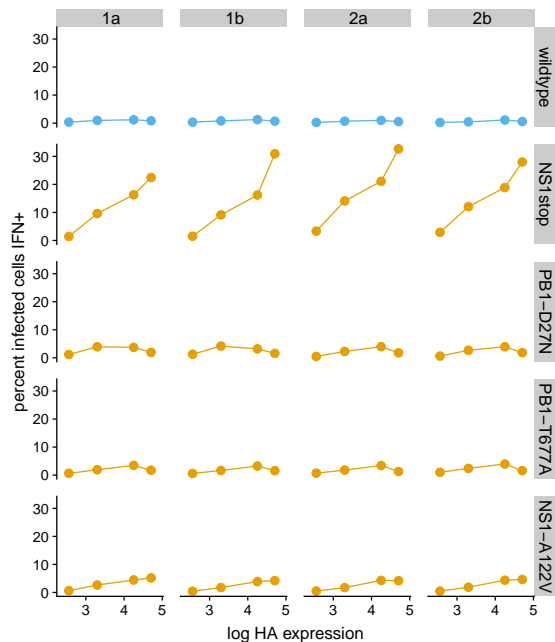


FIG S14 A more detailed version of the data summarized in Fig. 7. For each virus and replicate, we binned the infected cells in Fig. S12 into HA expression quartiles based on the flow cytometry measurements. We then calculated the percent of cells that were IFN+ in each quartile. The plots show the mean HA expression of the quartile versus the percent of cells that are IFN+. The results clearly show that for the NS1stop and to a lesser extent the NS1-A122V variants, more viral protein (higher HA signal) correlates with IFN induction. Fig. 7 summarizes these same data by simply showing the ratio of percent IFN+ between the highest and lowest quartile.

FILE S1 Sequences of the IFN reporters in Fig. 1A are at https://github.com/jbloomlab/IFNssorted_flu_single_cell/tree/master/paper/figures/IFN_stochastic/IFN_reporter/plasmids. This file is also available on Data Dryad Digital Repository at <https://doi.org/10.5061/dryad.nh053c6>.

FILE S2 Genbank files giving sequences of the wild-type and synonymously bar-coded viruses are at https://github.com/jbloomlab/IFNssorted_flu_single_cell/blob/master/data/flu_sequences/flu-wsn.gb and https://github.com/jbloomlab/IFNssorted_flu_single_cell/blob/master/data/flu_sequences/flu-wsn-double-syn.gb. This file is also available on Data Dryad Digital Repository at <https://doi.org/10.5061/dryad.nh053c6>.

FILE S3 A text file giving the primers used to amplify the influenza cDNAs for PacBio sequencing is at https://github.com/jbloomlab/IFNssorted_flu_single_cell/tree/master/paper/figures/WorkflowSchematic/PacBio_primer_list.txt. This file is also available on Data Dryad Digital Repository at <https://doi.org/10.5061/dryad.nh053c6>.

FILE S4 A CSV file giving the genotypes in Fig. 4 is at https://github.com/jbloomlab/IFNssorted_flu_single_cell/blob/master/paper/figures/single_cell_figures/genotypes.csv. This file is also available on Data Dryad Digital Repository at <https://doi.org/10.5061/dryad.nh053c6>.

FILE S5 A CSV file giving the viral mutations and related information in Fig. 5 is at https://github.com/jbloomlab/IFNssorted_flu_single_cell/blob/master/paper/figures/single_cell_figures/mutations.csv. This file is also available on Data Dryad Digital Repository at <https://doi.org/10.5061/dryad.nh053c6>.

FILE S6 Genbank plasmid maps for the mutant genes cloned into the pHW* bi-directional reverse genetics plasmid -(52) are at https://github.com/jbloomlab/IFNssorted_flu_single_cell/tree/master/paper/figures/FluVariantPlasmidMaps. This file is also available on Data Dryad Digital Repository at <https://doi.org/10.5061/dryad.nh053c6>.

FILE S7 The Jupyter notebook that analyzes the PacBio data is at https://github.com/jbloomlab/IFNsorted_flu_single_cell/blob/master/pacbio_analysis.ipynb. This file is also available on Data Dryad Digital Repository at <https://doi.org/10.5061/dryad.nh053c6>.

FILE S8 The Jupyter notebook that analyzes the annotated cell-gene matrix is at https://github.com/jbloomlab/IFNsorted_flu_single_cell/blob/master/monocle_analysis.ipynb. This file is also available on Data Dryad Digital Repository at <https://doi.org/10.5061/dryad.nh053c6>.